Charm physics with a Lattice QCD mixed action

Javier Ugarrio Muñoz

Under the Supervision of:
Carlos Pena Ruano

Departamento de Física Teórica
Universidad Autónoma de Madrid

Instituto de Física Teórica
UAM-CSIC

En memoria de mi madre.

Abstract

In this thesis we study a mixed-action Lattice QCD setup, which combines $N_f = 2 + 1$ $O(a)$-improved Wilson fermions and $N_f = 2 + 1 + 1$ Wilson twisted mass (Wtm) fermions at maximal twist in the valence. We take advantage of automatic $O(a)$ improvement in the valence sector to extract charm physics results without improvement coefficients.

Our results include the determination of the charm quark mass, as well as of the decay constants of the D and D_s mesons, relevant for electroweak leptonic decays. Quarkonium states are also studied. We carry out an analysis that focuses on controlling the statistical and systematic errors. Systematic effects are considered in the framework of Bayesian statistics. Different model parameterizations are taken into consideration to perform a model average. Our final results are among the most precise in the literature for computations employing Wilson-like fermions and will contribute significantly to the current world averages.

Resumen

En esta tesis estudiamos una configuración de acción mixta, que combina $N_f = 2+1$ fermiones Wilson mejorados a $O(a)$ y $N_f = 2+1+1$ fermiones Wilson twisted mass (Wtm) a twist máximo. Aprovechamos el mejorado a $O(a)$ automático en el sector de valencia para extraer resultados de física de charm sin coeficientes de mejora.

Nuestros resultados incluyen la determinación de la masa del quark charm, así como también las constantes de desintegración de los mesones D y D_s, relevantes para las desintegraciones electrodébiles leptónicas. También estudiamos estados de quarkonio. Consideramos efectos sistemáticos en un contexto de estadística Bayesiana. Se consideran diferentes parametrizaciones para efectuar una media de modelos. Nuestro resultados finales están entre los resultados más precisos de la literatura con cálculos que emplean fermiones Wilson-like y contribuirán significativamente a las medias mundiales actuales.

CONTENTS

1 INTRODUCTION

Quantum Field Theory (QFT) is the theoretical framework that describes fundamental forces and particles in terms of fields and symmetries by integrating naturally the principles from Special Relativity and Quantum Mechanics. QFT has proven to be extremely successful, although some aspects of it are yet to be explored, since, for example, a fully consistent QFT formulation for gravitational interactions has not been achieved yet. It can, however, describe electroweak and strong interactions, and it has led to numerous results that are in agreement with experimental observations.

The most succesful model for particle physics, based on QFT, is the Standard Model of Particle Physics (SM), a renormalizable theory described by the symmetry group $SU(3)_c \times SU(2)_L \times U(1)_Y$. It allows to explain the dynamics of the gauge fields, which describe the fundamental forces, and their interactions with the fermionic fields, which represent the matter content of the model and are categorized into quarks and leptons. The Standard Model contains 12 fermion fields in total: 6 quarks and 6 leptons, that are organized among 3 families, and 12 bosonic gauge fields as well: the photon, the Z boson, the $W^{\pm}$ bosons, and eight gluons. The latter are said to be the mediators of strong interactions, which, together with the quark fields, are described by the framework of Quantum Chromodynamics (QCD), the $SU(3)_c$ subgroup of the SM. This particular piece of the model will be of special interest in this Thesis.

QCD is an asymptotically free theory, which means that gauge interactions become weaker at high energies, whereas they become strongly coupled in the low-energy regime, *i.e.*, below energies of the order of the proton mass. In this regime, therefore, perturbative calculations break down and can no longer be relied upon. Furthermore, QCD exhibits non-perturbative phenomena such as confinement or spontaneous chiral symmetry breaking, having important implications such as the fact that quarks are not observed free in Nature, as they remain bound into mesons and baryons.

Beyond the fermions and gauge bonsons, the SM also includes a scalar field that generates the mass of the particles: the so-called Higgs field. According to the model, this field is coupled to the fermionic fields through Yukawa couplings, and when the Electroweak Spontaneous Symmetry Breaking mechanism takes place, a mass is generated for these fermions. After spontaneous symmetry breaking, mass

eigenstates for the quark fields are no longer eigenstates of the weak interactions. It leads to a constrained structure in the weak flavor-changing interactions for quarks. The Cabibbo–Kobayashi–Maskawa (CKM) matrix parametrizes the mixing in those interactions. The matrix presents a hierarchical structure, where off-diagonal matrix elements are suppressed. In addition, the Jarlskog invariant, which is related to CP violation in the Standard Model is far from being "of natural size". These issues may be addressed as a result of new Physics beyond the Standard Model.

The fact that the CKM matrix is a unitary matrix constrains the matrix elements that are represented by unitarity triangles. Therefore, inconsistencies in the CKM matrix can lead to New Physics beyond the Standard Model. Electroweak hadron decays provide a way to study Flavor Physics in the hadronic sector. These processes are used to measure CKM matrix elements and other observables regarding flavor physics.

The study of these phenomena requires the introduction of a non-perturbative framework for Quantum Field Theories. Lattice Field Theory is a non-pertubative regularization that allows to perform those computations. The idea was introduced by K. Wilson [1] and it is based on the space-time discretization and regularization of the fields on a lattice. This formalism opens the door to numerical simulations. However, Lattice QCD simulations are a multiscale problem, where energy scales vary from pion masses to B meson masses $140\,\mathrm{MeV} \lesssim \Lambda \lesssim 5\,\mathrm{GeV}$. Effective field theories such as Heavy Quark Effective Theory (HQET) or Chiral Perturbation Theory (χPT) are additional tools that combined to Lattice QCD provide physical results for non-perturbative observables.

We focus on the study of charm physics. We determine decay constants $f_{D_{(s)}}$, which play a role in leptonic decays of D and D_s mesons. Those decay constants parametrize the decay rates $\Gamma(D_{(s)} \to l\nu)$. Experimental measurements of the decay rates combined with lattice results allow the determination of the module of CKM matrix elements $V_{c,d}$ and $V_{c,s}$

$$\Gamma(D_{(s)} \to l\nu) = \frac{G_F^2}{8\pi} f_{D_{(s)}} m_l^2 M_{D_{(s)}} \left(1 - \frac{m_l^2}{M_{D_{(s)}}^2}\right)^2 \left|V_{c,d(s)}\right|^2 . \tag{1.1}$$

We introduce a mixed-action setup that focuses on the computation of heavy quark physics, while controlling the systematics. Our setup uses CLS ensembles [2] with open boundary conditions in the time direction, which allows to reach smaller lattice spacings while keeping autocorrelations under control. Computations with finer values of the lattice spacing are essential to study heavy quark physics. We use a Wilson twisted mass action in the valence sector to compute $O(a)$-improved quantities

without the need to include improvement coefficients, and therefore systematic effects are simplified.

We developed a Julia package called juobs for the computation of QCD observables based on the ADerrors library [3]. ADerrors simplifies the error propagation of complex functions, while keeping track of all the covariances and autocorrelations.

The Thesis is organized as follows: we introduce Lattice Field Theory in Chapter 2. We review some general contents and describe the regularizations that are used in our setup. In Chapter 3, we describe our mixed-action setup with $N_f = 2 + 1$ dynamical quarks and $N_f = 2 + 1 + 1$ quarks in the valence sector. General aspects about algorithms and computation of physical observables on the lattice are summarized in Chapter 4. We provide results for the leptonic decay constants and the charm quark mass in different renormalization schemes in Chapter 5. In this chapter, we describe the strategy followed to obtain continuum-limit results and the error estimation.

2 LATTICE REGULARIZATION

Lattice field theory is a general non-pertubative tool, which allows to address computations of physical quantities in a given gauge theory. In this chapter, we describe the theoretical aspects of the lattice regularization applied to Quantum Chromodynamics (QCD) as proposed by K. Wilson [1].

In order to define a quantum field theory, a regularization procedure is required. Lattice field theory defines the fields on a discrete space-time lattice, which provides an ultraviolet cutoff that does not rely on perturbation theory. The fields are defined on a finite lattice in a 4-dimensional asymmetrical hypercubical lattice of volume $V_4 = TL^3$, where T and L are the lengths in the the time and spatial directions respectively. Each position of space-time lattice can be expressed in terms of a vector of integers $n \in \mathbb{Z}^4$ as follows

$$x = (x_0, x_1, x_2, x_3) = a(n_0, n_1, n_2, n_3), \quad n_0 \in [0, T/a)\,,\ n_i \in [0, L/a)\,, \tag{2.1}$$

where a is the lattice spacing, that acts as an ultraviolet cutoff $\Lambda_{UV} = a^{-1}$. In sections 2.1 and 2.2 we describe the regularization of gauge and fermion fields on the lattice in the Euclidean space. We introduce two different regularizations for the fermion fields that will be relevant for our current setup.

In order to quantize the classical theory, we use the path integral formalism. In this framework, all the physical observables are computed in terms of Green functions. In Section 2.3, we describe how the path integral is regularized in Euclidean space. In the Euclidean space each field configuration in the path integral is weighted by a Boltzmann factor e^{-S_E} provided that $S_E > 0$, and therefore correlation functions can be computed using statistical mechanics methods such as Monte Carlo integration. Monte Carlo methods provide a numerical solution to the problem. A more detailed discussion about Monte Carlo simulations can be found in section 4.1. In section 2.4, we describe how to determine hadronic physical observables from Euclidean correlation functions, in particular two-point functions.

In section 2.5, we discuss the formulation of LQCD as an effective theory of continuum QCD and we sketch out how to define $O(a)$-improved renormalized observables, *i.e.*, observables that do not depend linearly on the ultraviolet cutoff.

2.1 GAUGE ACTION

In order to regularize a gauge theory, one should study gauge invariance in detail. Since fields at different points in the lattice transform differently under the gauge group, we need to introduce parallel transporters for the fields such that gauge invariance is preserved. This parallel transporters are the so-called Wilson lines and they allow to move the fields around, while preserving gauge invariance.

For a non-Abelian $SU(N)$ gauge group with generators $\frac{\lambda^a}{2}$, we have that a field, transforming in the fundamental representation, transforms under the group as

$$\phi(x) \to e^{i\alpha^a(x)\frac{\lambda^a}{2}}\phi(x), \tag{2.2}$$

where $\alpha^a(x)$ are the parameters that define the gauge transformation. So, if we try to compare the value of the field at two different points we find that it depends on the choice of local phases. We need a bi-local field $U(x,y)$, called Wilson line, which transforms as

$$U(x,y) \to e^{i\alpha^a(x)\frac{\lambda^a}{2}}U(x,y)e^{-i\alpha^b(y)\frac{\lambda^b}{2}}. \tag{2.3}$$

The key point is that now, we can construct expressions such as

$$U(x,y)\phi(x) - \phi(y) \to e^{i\alpha^a(y)\frac{\lambda^a}{2}}[U(x,y)\phi(x) - \phi(y)], \tag{2.4}$$

and therefore by taking two points infinitesimally closed $y = x + \delta x$, we can turn this difference into a derivative. It allows to define a covariant derivative

$$D_\mu\phi(x) \equiv \lim_{\delta x^\mu \to 0} \frac{U(x, x+\delta x_\mu)\phi(x+\delta x_\mu) - \phi(x)}{\delta x^\mu}, \tag{2.5}$$

which transforms as a conventional covariant derivative $D_\mu\phi(x) \to e^{i\alpha^a(x)\frac{\lambda^a}{2}}D_\mu\phi(x)$.

Wilson lines can be expressed in terms of the gauge field A^a_μ, along a curve $\mathcal{C}$ between points x and y

$$U(x,y) = P\exp\left(ig\int_{\mathcal{C}} A^a_\mu(z)\frac{\lambda^a}{2}\mathrm{d}z_\mu\right), \tag{2.6}$$

where P is the path-ordering operator. By applying the fundamental theorem of calculus is easy to check that Wilson lines transform as desired under gauge group transformations.

Once we have defined a Wilson lines for a $SU(N)$ gauge group and we have shown the relation between the Wilson line U and the gauge fields A^a_μ, we can look

at the discretization process of a gauge theory. On a lattice, we can define a Wilson link between two nearest-neighbour sites n and $n+\hat{\mu}$ as

$$U_\mu(n) = P\exp\left(ia\int_{n\to n+\hat{\mu}} A^a_\mu(n)\frac{\lambda^a}{2}\right). \tag{2.7}$$

To construct the pure gauge action we need a gauge invariant object constructed out of Wilson links. From the transformation property of Wilson links we know that any closed loop of links will be gauge invariant. The first non-trivial Wilson loop that we can construct on a lattice is the so-called plaquette, obtained by moving arround an elementary square on the lattice, viz.

$$U_{\mu\nu}(n) = U^\dagger_\nu(n)U^\dagger_\mu(n+\hat{\nu})U_\nu(n+\hat{\mu})U_\mu(n). \tag{2.8}$$

If the plaquette is expanded for small values of the lattice spacing a, it is found to be related to the field strength[1] $\mathbf{F}_{\mu\nu}$ as

$$U_{\mu\nu}(n) = e^{ia^2\mathbf{F}_{\mu\nu}(n)+O(a^3)}, \tag{2.9}$$

The plaquette action [1] provides a simple regularization of the pure gauge action

$$\begin{aligned} S_G[U] = \frac{\beta}{2N}\sum_{n,\mu\nu}\mathrm{Re}(\mathrm{tr}(\mathbb{1}-U_{\mu\nu}(n))) &\overset{a\to 0}{\to} \frac{a^4}{2g^2}\sum_{n,\mu\nu}\mathrm{tr}\left(\mathbf{F}^2_{\mu\nu}(n)\right)+O(a^6) \\ &\overset{a=0}{=} \frac{1}{2g^2}\int \mathrm{d}^4\mathrm{x}\,\mathrm{tr}\left(\mathbf{F}^2_{\mu\nu}(x)\right), \quad \beta\equiv\frac{2N}{g^2}. \end{aligned} \tag{2.10}$$

Nevertheless, other choices for the simplest Yang-Mills action are possible which keep the correct continuum limit such as the Lüscher-Weisz action [4].

In addition, a covariant derivative on a lattice can be defined from the expression (Eq. 2.5) using a forward derivative prescription

$$\nabla_\mu\phi(n) = \frac{1}{a}\left(U_\mu(n)\phi(n+\hat{\mu})-\phi(n)\right). \tag{2.11}$$

Note that this expression is not unique and one could have used another prescription for the derivative, in the form of a backward derivative.

$$\nabla^*_\mu\phi(n) = \frac{1}{a}\left(\phi(n)-U^\dagger_\mu(n-\hat{\mu})\phi(n-\hat{\mu})\right). \tag{2.12}$$

[1] The field strength tensor is an element of the Lie algebra, so it can be decomposed as $\mathbf{F}_{\mu\nu}(x) = \sum_a \frac{\lambda^a}{2}F^a_{\mu\nu}(x)$.

In the continuum the forward and backward convariant derivatives are related to the convariant derivative D_μ such that

$$\begin{aligned} \nabla_\mu \phi(n) &\overset{a\to 0}{\to} D_\mu \phi(n + a\hat{\mu}/2), \\ \nabla^*_\mu \phi(n) &\overset{a\to 0}{\to} D_\mu \phi(n - a\hat{\mu}/2). \end{aligned} \tag{2.13}$$

A symmetric convariant derivative can be introduced such that

$$\frac{1}{2}(\nabla_\mu + \nabla^*_\mu)\phi(n) \overset{a\to 0}{\to} D_\mu \phi(n). \tag{2.14}$$

In a similar way, ordinary lattice derivatives can be defined as follows

$$\begin{aligned} \partial_\mu \phi(n) &= \frac{1}{a}\left(\phi(n + \hat{\mu}) - \phi(n)\right), \\ \partial^*_\mu \phi(n) &= \frac{1}{a}\left(\phi(n) - \phi(n - \hat{\mu})\right). \end{aligned} \tag{2.15}$$

2.2 FERMION ACTION

In order to formulate QCD on a lattice, we need to properly formulate fermion fields on a discretized space-time. At first, we can focus on regularizing a free fermion theory. Then, we can charge those fermions under some symmetry group and promote it to a gauge symmetry as usual. Thus, the symmetry can be promoted replacing derivatives by covariant derivatives, which are described in terms of Wilson links Eq. (2.11).

2.2.1 Naive regularization

As first approximation, a free fermion action in the Euclidean space can be naively discretized as

$$\begin{aligned} S_F[\psi, \bar{\psi}] &= a^4 \sum_n \bar{\psi}(n) \left[\frac{1}{2}\gamma_\mu(\partial_\mu + \partial^*_\mu) + M\right] \psi(n) \\ &= a^4 \sum_{n,m,\alpha,\beta} \bar{\psi}_\alpha(n) K_{\alpha,\beta}(n,m) \psi_\beta(m), \\ K_{\alpha,\beta}(n,m) &\equiv \sum_\mu \frac{1}{2a}(\gamma_\mu)_{\alpha\beta}\left[\delta_{m,n+\hat{\mu}} - \delta_{m,n-\hat{\mu}}\right] + M\delta_{m,n}\delta_{\alpha,\beta}, \end{aligned} \tag{2.16}$$

where the symmetrized derivative has been taken.

The path integral can be easily integrated to obtain the generating functional $Z[\eta, \bar{\eta}]$

$$Z[\eta, \bar{\eta}] = \det K \exp\left[a^{-4} \sum_{n,m} \bar{\eta}(n) K^{-1}(n,m) \eta(m)\right], \tag{2.17}$$

and therefore the fermion propagator in this notation is defined by

$$S(n,m) = \langle \psi(n) \bar{\psi}(m) \rangle = K^{-1}(n,m). \tag{2.18}$$

The operator $K(n,m)$ is easily inverted after applying a Fourier transform to momentum space

$$K(k,-p) = \sum_{n,m} e^{ia(k\cdot m - p\cdot n)} K(n,m) \Rightarrow S(k) = \frac{M - i\sum_\mu \gamma_\mu \sin(ak_\mu)/a}{M^2 + \sum_\mu \sin^2(ak_\mu)/a^2}. \tag{2.19}$$

Notice that translational invariance implies that one can just work at $p = k$ on the r.h.s of the equation.

The fermion propagator converges properly to the continuum limit in the center of the Brillouin zone

$$S(k) = \frac{-i\gamma_\mu k_\mu + M}{k^2 + M^2} + O(a^2), \tag{2.20}$$

and it has a pole at $k_4 = i\sqrt{\vec{k}^2 + M^2}$ as we expect from the continuum theory. However, other 15 poles appear in the corners of the Brilloiun zone. Thus, 15 unphysical particles called doublers appear on the lattice that do not decouple in the continuum limit. The Nielsen-Ninomiya no-go theorem for chiral fermions [5] states those unphysical states can not be removed without spoiling properties of the theory such as, the chiral symmetry.

2.2.2 Wilson fermions

For that reason, a different way to discretize fermions on the lattice is needed. The simplest one is the so-called Wilson fermion regularization [6]. It consists of adding an irrelevant term, which vanishes when $a \to 0$, to the naive action regularization.

This term can be understood as a momentum-dependent mass term, which rises the masses of the doublers to values of the order of the cutoff.

$$\begin{aligned} S_F^{(W)} &= a^4 \sum_n \bar{\psi} \left[\frac{1}{2} \gamma_\mu (\partial_\mu + \partial_\mu^*) + M - \frac{a}{2} \partial_\mu \partial_\mu^* \right] \psi(n) \\ &= a^4 \sum_{n,m,\alpha,\beta} \bar{\psi}_\alpha(n) K^W_{\alpha,\beta}(n,m) \psi_\beta(m), \\ K^W_{\alpha,\beta}(n,m) &\equiv \sum_\mu \frac{1}{2a} \left[(\gamma_\mu - 1)_{\alpha\beta} \delta_{m,n+\hat{\mu}} - (\gamma_\mu + 1)_{\alpha\beta} \delta_{m,n-\hat{\mu}} \right] \\ &\quad + (M + 4a^{-1}) \delta_{m,n} \delta_{\alpha,\beta}. \end{aligned} \tag{2.21}$$

This action leads to the following propagator

$$S(k) = \frac{\mathcal{M}(k) - i \sum_\mu \gamma_\mu \sin(a k_\mu)/a}{\mathcal{M}^2(k) + \sum_\mu \sin^2(a k_\mu)/a^2}, \tag{2.22}$$

with

$$\mathcal{M}(k) \equiv M + \frac{2}{a} \sum_\mu \sin^2(a k_\mu/2), \tag{2.23}$$

which has just one particle pole within the first Brillouin zone.

The full fermion action of Wilson fermions in presence of a gauge field is accomplished by substituting the derivatives for covariant derivatives

$$\begin{aligned} S_F[\psi, \bar{\psi}, U] &= a^4 \sum_n \bar{\psi}(n) \left[D_W + M \right] \psi(n), \\ D_W &= \frac{1}{2} \left[\gamma_\mu (\nabla_\mu + \nabla_\mu^*) - a \nabla_\mu \nabla_\mu^* \right]. \end{aligned} \tag{2.24}$$

The main shortcoming of the Wilson regularization is that it breaks axial symmetry in the chiral limit explicitly, which will introduce complications in the quantum theory. New operators that do not preserve axial symmetry will appear in the renormalization process. In Section 2.5 we describe those terms and we discuss the construction of the effective theory.

2.2.3 Twisted mass fermions

As we have seen before, the Wilson fermion regularization introduces several complications. The Wilson term breaks explicitly the axial symmetry in the chiral limit. As a result of this explicit symmetry breaking new operators, which respect the symmetry of the regularized theory, arise. Physically, quark masses are no longer renormalized multiplicatively. On the other hand, the Wilson-Dirac operator is not protected against eigenvalues below the quark mass. It has been shown that configurations

with low-energy eigenvalues introduce instabilities in the simulations [7]. In this section, we summarize some aspects of the twisted mass regularization [8] (see [9] for a detailed review). We will review the construction for two degenerate flavor for simplicity reasons. The results can be generalized for any multiplet.

As we have seen before, the standard Wilson action in Euclidean space is given by Eq. (2.24). More generally, the theory can be regularized substituting the standard Wilson operator D_W for the twisted Wilson operator that depends on a twist angle ω which parametrizes a family of regularizations, which have the same continuum limit.

$$D_{Wtm} = \frac{1}{2}\left[\gamma_\mu(\nabla_\mu + \nabla^*_\mu) - a e^{i\omega\gamma_5\tau_3}\nabla_\mu\nabla^*_\mu\right]. \tag{2.25}$$

The choice $\omega = 0$ corresponds to the standard Wilson regularization and $\omega = \pi/2$ corresponds to the so-called full or maximal twist case. It is easy to see that a twisted basis $\{\chi, \bar{\chi}\}$ can be defined performing a chiral rotation which mixes isospin components as

$$\psi = \exp\left(-i\omega\gamma_5\tau_3/2\right)\chi, \quad \bar{\psi} = \bar{\chi}\exp\left(-i\omega\gamma_5\tau_3/2\right). \tag{2.26}$$

Thus, in the twisted basis the fermion action may be described by

$$S_F[\chi, \bar{\chi}, U] = a^4 \sum_x \bar{\chi}(x)(D_W + m_0 + i\mu_0\gamma_5\tau_3)\chi(x), \tag{2.27}$$

where the bare untwisted mass m_0 and the bare twisted mass μ_0 fulfill

$$m_0 = M\cos\omega \quad , \quad \mu_0 = M\sin\omega, \tag{2.28}$$

and $M = \sqrt{m_0^2 + \mu_0^2}$ is the so-called polar mass. As we have mentioned before, the Wilson term breaks axial symmetry explicitly even in the massless limit. Considering a degenerate doublet, the theory is symmetric under the global group $SU(2)_V \otimes SU(2)_A$. For $\omega = 0$, the Wilson term spoils the axial symmetry and the symmetry group reduces to $SU(2)_V$. Twisted mass regularization at $\omega = \pi/2$ breaks down the group into $SU(2)_V \to [U(1)_A]_1 \otimes [U(1)_A]_2 \otimes [U(1)_V]_3$.

$$[U(1)_A]_a : \begin{cases} \psi(x) \to \exp\left(i\alpha^a_A\gamma_5\frac{\tau^a}{2}\right)\psi(x), & a = 1,2 \\ \bar{\psi}(x) \to \bar{\psi}(x)\exp\left(i\alpha^a_A\gamma_5\frac{\tau^a}{2}\right), & a = 1,2 \end{cases} \tag{2.29}$$

and

$$[U(1)_V]_3 : \begin{cases} \psi(x) \to \exp\left(i\alpha^3_V\frac{\tau^3}{2}\right)\psi(x) \\ \bar{\psi}(x) \to \bar{\psi}(x)\exp\left(-i\alpha^3_V\frac{\tau^3}{2}\right) \end{cases} \tag{2.30}$$

Therefore, using Wilson twisted mass (Wtm) at full twist axial symmetries are not completely broken. As a consequence, the symmetry protects the mass term from additive renormalization in contrast with Wilson fermions.

The continuum action at maximal twist is symmetric under the discrete symmetry $R_5^{1,2}$

$$R_5^{1,2} : \begin{cases} \bar{\chi} \to i\bar{\chi}\gamma_5\tau^{1,2} \\ \chi \to i\gamma_5\tau^{1,2}\chi \end{cases} \tag{2.31}$$

that will be important for the Symanzik's $O(a)$-improvement program in Section 2.5. Correlation functions that are even under the discrete transformation $R_5^{1,2}$ are automatically $O(a)$- improved. As will be explained later, the twisted mass regularization can be extended to non-degenerate fermions, maintaining the benefits of this regularization.

2.3 PATH INTEGRAL REGULARIZATION

In the path integral formalism, all physical observables are computed in terms of expectation values of operators. The expectation value of a general multilocal operator $\mathcal{O}(x_1, \ldots, x_n)$ reads

$$\langle \mathcal{O}(x_1, \ldots, x_n) \rangle = \frac{1}{Z} \int \mathcal{D}[\psi, \bar{\psi}, U]\, \mathcal{O}(x_1, \ldots, x_n) e^{-S[\psi,\bar{\psi},U]}, \tag{2.32}$$

where the integration measure $\mathcal{D}[\psi, \bar{\psi}, U]$ is the product over all gluonic and fermionic configurations. The Euclidean partition function $Z = \int \mathcal{D}[\psi, \bar{\psi}, U]\, e^{-S[\psi,\bar{\psi},U]}$ guarantees that the expression has the correct normalization. In Euclidean space, the expression is analogous to statistical mechanics where the Boltzmann factor is given by the action $e^{-S[\psi,\bar{\psi},U]}$.

In order to simplify the expression, the fermion contribution can be integrated out so the path integral is defined in terms of the Wilson links. We split the action into two contributions: the pure gauge action and the fermionic action $S[\psi, \bar{\psi}, U] = S_G[U] + S_F[\psi, \bar{\psi}, U]$. So, the expectation is written as

$$\begin{aligned} \langle \mathcal{O}(x_1, \ldots, x_n) \rangle &= \frac{1}{Z} \int \mathcal{D}[U]\, e^{-S_G[U]} Z_F[U] \left[\frac{1}{Z_F[U]} \int \mathcal{D}[\psi, \bar{\psi}]\, e^{-S_F[\psi,\bar{\psi},U]} \mathcal{O}(x_1, \ldots, x_n) \right] \\ &= \frac{1}{Z} \int \mathcal{D}[U]\, e^{-S_G[U]} Z_F[U]\, \langle \mathcal{O}(x_1, \ldots, x_n) \rangle_F \,, \end{aligned} \tag{2.33}$$

where Z_F contains the fermionic contribution to the partition function. The Berezin integration over the fermion fields leads to a fermion determinant

$$Z_F[U] = \int \mathcal{D}[\psi, \bar{\psi}]\, e^{-S_F[\psi,\bar{\psi},U]} = \prod_f \det(D_f), \tag{2.34}$$

where D_f is the Dirac operator that defines the fermion action for each flavor[2]. The fermion determinant can be expressed as a effective fermion action S_{eff}

$$\langle \mathcal{O}(x_1, \ldots, x_n) \rangle = \frac{1}{Z} \int \mathcal{D}[U]\, \langle \mathcal{O}(x_1, \ldots, x_n) \rangle_F\, e^{-S_G[U] - S_{\text{eff}}[U]}, \tag{2.35}$$

$$Z = \int \mathcal{D}[U]\, e^{-S_G[U] - S_{\text{eff}}[U]}, \tag{2.36}$$

$$S_{\text{eff}}[U] = -\sum_f \ln \det(D_f), \tag{2.37}$$

$\mathcal{O}(x_1, \ldots, x_n)$ may, in general contain both gluon and quark fields the latter of which give rise to propagators in $\langle \mathcal{O}(x_1, \ldots, x_n) \rangle_F$ via Wick contractions. We express the fermion determinant for a degenerate doublet using the two fermion regularizations introduced in the previous section. The fermionic effective action for Wilson fermions reads

$$S^W_{\text{eff}}[U] = -\ln(\det D_m)^2 = -\ln \det(D_m^\dagger D_m), \tag{2.38}$$

where the operator D_m is the standard Wilson-Dirac operator with the mass term $D_m = D_W + m$. We use γ_5-hermicity[3] of the Wilson-Dirac operator to simplify the fermion determinant, whereas for a doublet of twisted mass fermions we get

$$S^{\text{tm}}_{\text{eff}}[U] = -\ln \det\left((D_m + i\gamma_5\mu_0)(D_m - i\gamma_5\mu_0)\right) = -\ln \det(D_m^\dagger D_m + \mu_0^2). \tag{2.39}$$

Notice that the transformations Eq. (2.26) leave the integration measurement invariant since the transformation matrices belong to the special unitary group. Therefore, the fermion determinant can be computed by integrating over the fermion fields in the twisted basis $\{\chi, \bar{\chi}\}$.

Once the path integral is expressed in terms of the gauge links, a prescription for the gauge field is required to give the path integral formulation a meaning on a lattice. For a compact Lie group the path integral can be defined as

$$\int \mathcal{D}U = \prod_{x,\mu} \int \mathrm{d}U_\mu(x), \tag{2.40}$$

[2] The fermion action is defined as $S_F = \sum_f \int \mathrm{d}^4\mathrm{x}\, \bar{\psi}_f(x) D_f \psi_f(x)$.

[3] $D_W^\dagger = \gamma_5 D_W \gamma_5$.

where $\mathrm{d}U$ is a volume element in group space for a given link. We want the partition function Z to be gauge invariant. The measure that is invariant under Eq. (2.3) is known as Haar measure

$$\mathrm{d}U = \nu\sqrt{\det g}\prod_a \mathrm{d}\alpha^a, \tag{2.41}$$

where g is the metric associated to the compact Lie group, α^a are the coordinates on the group, and ν is some normalization factor such that $\int \mathcal{D}U = 1$. Gauge fixing is not needed in the lattice regularization, since there is a finite number of space-time points and therefore the volume of the gauge group is finite and the Haar measure can be normalized properly.

If the Euclidean the exponential factor is positive definite. Hence, one can interpret it as a probability distribution function. Nevertheless, Wilson fermions contain low-energy modes that spoils this property. Generally, the path integral can be estimated using Monte Carlo integration in the Euclidean space. The field configurations are generated given the following distribution

$$P[U] \sim \prod_f \det(D_f)\, e^{-S_G[U]} = e^{-S_G[U]-S_{\text{eff}}[U]}. \tag{2.42}$$

An algorithm that generates configurations is needed. The algorithm samples the full parameter space following the probability distribution function. Unlike the gauge action S_G, the fermionic effective action S_{eff} is non-local, so the algorithm has to be efficient dealing with non-local couplings between links. The algorithm also need to address the low-energy modes that lead to exceptional configurations. The details of configuration generation are explained in Section 4.1.

2.4 EUCLIDEAN CORRELATION FUNCTIONS

In order to extract physical observables, we compute Euclidean correlation functions. In this section we will show the relation between Euclidean correlation functions and hadronic matrix elements. We will focus on two-point correlation functions. We consider a lattice with time extension T and spatial volume L^3, with some open conditions on the Euclidean time direction and periodic boundary conditions on the spatial volume. We consider a local fermionic operator of the form

$$O_i^{q,r}(x) = \bar{\psi}^q(x)\Gamma_i\psi^r(x), \tag{2.43}$$

where Γ_i is a spin matrix, and spin and color indices are traced over. A general on-shell two point function can be constructed with those fermionic operators on the lattice

$$\langle O_j^{r,q}(x) O_i^{q,r}(y)\rangle = \frac{1}{Z}\langle \Phi_f | e^{-(T-x_0)H} O_j^{r,q}(\vec{x}) e^{-(x_0-y_0)H} O_i^{q,r}(\vec{y}) e^{-y_0 H} |\Phi_i\rangle\,, \quad (2.44)$$

where the states $|\Phi_i\rangle$ and $|\Phi_f\rangle$ denote the initial and final boundary states respectively. The partition function Z for large lattice time extensions T becomes

$$Z = \sum_{\vec{p},n} \frac{1}{2E_n(\vec{p})L^3} \langle \Phi_f|\vec{p},n\rangle\, e^{-TE_n(\vec{p})}\, \langle \vec{p},n|\Phi_i\rangle \overset{T\to\infty}{\to} \langle \Phi_f|0\rangle\langle 0|\Phi_i\rangle\, e^{-TE_0}. \quad (2.45)$$

The states[4] $|\vec{p},n\rangle$ represent a complete basis of the Fock space that are eigenstates of the Hamiltonian $H|\vec{p},n\rangle = E_n(\vec{p})|\vec{p},n\rangle$. By assuming that the local operators are on the bulk, $y_0 \gg 1$ and $T - x_0 \gg 1$, the expression can be simplified to the leading contribution

$$\begin{aligned}\langle O_j^{r,q}(x) O_i^{q,\,r}(y)\rangle \approx \frac{1}{Z}\sum_{\vec{p},n}\frac{1}{2E_n(\vec{p})L^3}\langle 0|O_j^{r,q}(\vec{x})|\vec{p},n\rangle \times \\ \langle \vec{p},n|O_i^{q,r}(\vec{y})|0\rangle\, e^{-(x_0-y_0)E_n(\vec{p})-(T-x_0+y_0)E_0}.\end{aligned} \quad (2.46)$$

After applying spatial translation to the local operators we get

$$\langle O_j^{r,q}(x) O_i^{q,r}(y)\rangle \approx \sum_{\vec{p},n}\frac{e^{i\vec{p}(\vec{x}-\vec{y})}}{2E_n(\vec{p})L^3}\langle 0|O_j^{r,q}|\vec{p},n\rangle\langle \vec{p},n|O_i^{q,r}|0\rangle\, e^{-(x_0-y_0)(E_n(\vec{p})-E_0)}. \quad (2.47)$$

Then, it is easy to see that the spatial volume average projects the states onto zero-momentum states.

$$\begin{aligned}\frac{1}{L^3}\sum_{\vec{x},\vec{y}}\langle O_j^{r,q}(x) O_i^{q,r}(y)\rangle &\approx \sum_{\vec{p},n}\frac{\delta_{\vec{p},0}}{2E_n(\vec{p})}\langle 0|O_j^{r,q}|\vec{p},n\rangle\langle \vec{p},n|O_i^{q,r}|0\rangle\, e^{-(x_0-y_0)\tilde{E}_n(\vec{p})} \\ &= \sum_n \frac{1}{2E_n(\vec{0})}\langle 0|O_j^{r,q}|\vec{0},n\rangle\langle \vec{0},n|O_i^{q,r}|0\rangle\, e^{-(x_0-y_0)\tilde{E}_n(\vec{0})},\end{aligned} \quad (2.48)$$

[4] The states are normalized with the standard relativistic normalization $\langle \vec{q},m|\vec{p},n\rangle = 2E_n(\vec{p})L^3\delta_{n,m}\delta(\vec{p}-\vec{q})$

where the subtracted energy is defined such that $\tilde{E}_n(\vec{p}) \equiv E_n(\vec{p}) - E_0$. Using relativistic normalization of one-particle states

$$\frac{1}{L^3}\sum_{\vec{x},\vec{y}} \langle O_j^{r,q}(x) O_i^{q,r}(y)\rangle \approx L^3 \sum_n \langle 0|O_j^{r,q}|\phi_n\rangle \langle \phi_n|O_i^{q,r}|0\rangle \, e^{-(x_0-y_0)\tilde{E}_n(\vec{0})}. \tag{2.49}$$

The spectral decomposition of two-point correlation function can be used to determine different hadronic matrix elements and masses. We now introduce the notation for the correlation functions that we will use in Chapter 4 in order to sketch out how to extract those quantities.

$$f^{q,r}_{X,Y}(x_0,y_0) = \frac{a^6}{L^3}\sum_{\vec{x},\vec{y}} \langle X^{q,r}(x) Y^{r,q}(y)\rangle = a^6 L^3 \sum_n \langle 0|X^{q,r}|n\rangle \langle n|Y^{r,q}|0\rangle \, e^{-(x_0-y_0)\tilde{E}_n(\vec{0})}, \tag{2.50}$$

where the superscripts denotes flavor. X and Y represent different Dirac bilinears (see Appendix A). Hence, by studying the correlators at large time extensions $(x_0 - y_0) \to \infty$, we get the ground state contribution from which we can extract spectral quantities. For instance, pion states can be studied by computing light-light correlators.

$$f^{l,l}_{P,P}(x_0,y_0) \approx a^6 L^3 \langle 0|P^{l,l}|\pi\rangle \langle \pi|P^{l,l}|0\rangle \, e^{-(x_0-y_0)M_\pi}, \tag{2.51}$$

$$\frac{f^{l,l}_{A_0,P}(x_0,y_0)}{\sqrt{f^{l,l}_{P,P}(T-y_0,y_0)}} \approx a^3 L^{3/2} \left|\langle 0|A_0^{l,l}|\pi\rangle\right| e^{-(x_0-T/2)M_\pi}. \tag{2.52}$$

A detailed discussion on observables computation will be presented in Chapter 4, where we explain how to determine each fermionic observable that take part in the analysis through two-point correlators $f^{q,r}_{X,Y}(x_0,y_0)$.

2.5 RENOMALIZATION AND SYMANZIK'S $\mathcal{O}(a)$-IMPROVEMENT

To renormalize the theory we have to take into consideration the symmetries of the action. Since operators will mix with each other in the renormalization process, unless symmetry prevents them to.

Counterterms with dimension 4 or less will contribute to the renormalization of the action.

$$\mathcal{L}_R = \mathcal{L}_{\text{bare}} + \mathcal{L}_{\text{ct}}, \tag{2.53}$$

$$\mathcal{L}_{\text{ct}} = \textstyle\sum_i c_i \mathcal{O}_k^i a^{k-4}, \quad \dim(\mathcal{O}_k) = k. \tag{2.54}$$

In lattice simulations where continuum extrapolation is of crucial relevance to relate numerical simulations with experimental results. In practice, the continuum limit is taken performing lattice simulations at different values of the lattice spacing a, and then the limit is obtained by fitting the points and extrapolating to the continuum. The crucial tool under this procedure is Symanzik effective theory [10, 11], which describes the cutoff dependence of correlation functions. It provides a well-defined process both to parametrize the dependence on the lattice spacing, and to subtract the leading cutoff effects, resulting in better continuum extrapolations for physical quantities.

These counterterms can be chosen to cancel the linear contributions of the cutoff. Operators of dimension $d \geq 5$, called irrelevant operators, can be included in the effective theory. Although they do not contribute to the renormalized theory when the cutoff is removed, they can modify the dependence of the ultraviolet cutoff on some quantities.

The lattice field theory can be described by an effective theory, which at first order becomes the continuum QCD theory. The form of the effective theory is fixed by the symmetries of the lattice theory. Thus, in the effective theory the action is expanded in a power series in the lattice spacing a up to logarithmic corrections

$$S_{\text{eff}} = S_0 + aS_1 + a^2 S_2 + \ldots, \tag{2.55}$$

where S_0 is the action of continuum QCD and S_i are the terms given by actions of dimension $d \geq 5$. Higher-dimension terms provide cutoff contributions to the action and they vanish in the continuum limit, where the regulator is removed. Each contribution to the action S_k is parametrized with different coefficients c_i such that

$$S_k = \int \mathrm{d}^4\mathrm{x} \sum_i c_i \mathcal{O}_k^i(x), \quad \dim(\mathcal{O}_k) = 4 + k. \tag{2.56}$$

Similarly, cutoff effects also affect multilocal operators. A generic local operator made of some quark and gluon fields on the lattice is represented in the effective theory by an effective field of the form

$$\mathcal{O}_{\text{eff}}(x) = \mathcal{O}_0(x) + a\mathcal{O}_1(x) + a^2\mathcal{O}_2(x) + \ldots, \tag{2.57}$$

where the fields $\mathcal{O}_i$ have the appropriate dimension and the same quantum numbers as the lattice field.

In the effective theory up to $O(a)$, the correlation function will be described by

$$\begin{aligned}\langle \mathcal{O}_{\text{eff}}(x_1)\dots\mathcal{O}_{\text{eff}}(x_n)\rangle = \langle \mathcal{O}_0(x_1)\dots\mathcal{O}_0(x_n)\rangle_0 - a\ \langle \mathcal{O}_0(x_1)\dots\mathcal{O}_0(x_n)S_1\rangle_0 \\ +a\sum_i^n \langle \mathcal{O}_0(x_1)\dots\mathcal{O}_1(x_i)\dots\mathcal{O}_0(x_n)\rangle_0 + O(a^2),\end{aligned} \tag{2.58}$$

where vacuum expectation values are taken in the continuum theory.

Wilson fermions

Since axial symmetry in the chiral limit protects mass terms from additive renormalization, this symmetry breaking will introduce a new counterterm when renormalizing the theory [12]

$$\mathcal{L}_{\text{c.t}} = \frac{c(g_0^2)}{a}\bar{\psi}\psi \equiv m_{\text{cr}}(g_0^2, a)\bar{\psi}\psi, \tag{2.59}$$

which introduces a critical mass, *i.e.* a linearly divergent term in the cutoff that has to be tuned to renormalize the theory.

$$m_R = Z_m(g_0^2, a)(m - m_{\text{cr}}(g_0^2, a)). \tag{2.60}$$

This phenomenon is analogous to what happens on scalar theories, which do not have any symmetry which protects the mass term. As a consequence of that, the mass term is no longer multiplicatively renormalized: a linear divergence arises from relevant operators that mix with the mass term.

For Wilson fermions, there are three dimension-5 operators which respect the symmetries of the regularized theory, which are

$$\mathcal{O}_1^1 = i\bar{\psi}\sigma_{\mu\nu}F_{\mu\nu}\psi, \tag{2.61}$$

$$\mathcal{O}_1^2 = m_q \text{tr}\{F_{\mu\nu}F_{\mu\nu}\}, \tag{2.62}$$

$$\mathcal{O}_1^3 = m_q^2\bar{\psi}\psi. \tag{2.63}$$

Effects of operators $\mathcal{O}^2$ and $\mathcal{O}^3$ can be reabsorbed in the definitions of coupling constant and renormalized masses, respectively. One can define the renormalized $O(a)$ improved masses and coupling constant tanking into account the counterterms

$$g_R^2 = Z_g g_0^2(1 + b_g a m_q), \tag{2.64}$$

$$m_R = Z_m m_q(1 + b_m a m_q), \tag{2.65}$$

where b_g and b_m are improvement coefficients and m_q is defined

$$m_q = m_0 - m_{\rm cr}. \tag{2.66}$$

There is just one additional term to the action, the so-called Clover term [13]

$$S_1 = \frac{i}{4}\int \mathrm{d}^4\mathrm{x}\, c_{\rm sw}\bar{\psi}(x)\sigma_{\mu\nu}F_{\mu\nu}(x)\psi(x), \tag{2.67}$$

where $c_{\rm sw}$ is the Sheikholeslami-Wohlert coefficient.

Wilson twisted mass fermions

A technical complication is that improvement coefficients are not known a priori and they must be tuned using either perturbation theory or lattice simulations. In practice, $O(a)$ improved Wilson fermions require several improvement coefficients and as we will see twisted mass regularization [14, 15] provides a way to extract some correlation functions automatically improved even if the theory is not $O(a)$ improved. On account of this, Wilson twisted mass (Wtm) requires the computation of less (or none at all) improvement coefficients in order to ensure an $O(a^2)$ scaling of physical quantities towards the continuum.

At full twist axial and vector symmetries are not completely broken as explained above. The charged axial symmetry in the chiral limit $[U(1)_A]_{1,2}$ prevents the twisted mass term to mix under renormalization with other relevant operators, and therefore the twisted mass renormalizes multiplicatively

$$\mu_R = Z_\mu \mu_0. \tag{2.68}$$

As a consequence, the symmetry protects the mass term from additive renormalization in contrast with Wilson fermions. However, the determination of $m_{\rm cr}$ is still required to renormalize the action. Maximal twist is obtained when the renormalized mass is completely given by the twisted mass term, *i.e.*, the renormalized twist angle is $\omega_R = \pi/2$. It implies that the renormalized untwisted mass vanishes $m_R = Z_m(m_0 - m_{\rm cr}) = 0$.

$$\tan\omega_R = \frac{\mu_R}{m_R}. \tag{2.69}$$

On the other hand, the isospin symmetry and parity are broken by the Wilson term. Hence, the neutral and charged pions are no longer degenerate in the effective theory. However, the mass splitting is given by $O(a^2)$ terms.

For Wilson twisted mass fermions at full twist, there are two dimension-5 operators that contribute to the effective action

$$\mathcal{O}_1^1 = i\bar{\chi}\sigma_{\mu\nu}F_{\mu\nu}\chi, \tag{2.70}$$

$$\mathcal{O}_1^2 = \mu_0^2\bar{\chi}\chi. \tag{2.71}$$

The operator $\mathcal{O}^2$ can be reabsorbed in the definition of the renormalized untwisted mass, whereas $\mathcal{O}^1$ provides the standard Clover term. The continuum action is even under the symmetry $R_5^{1,2}$ Eq. (2.31), whereas dimension-5 operators that contribute to the action are odd under that symmetry

$$S_0 \to S_0, \quad S_1 \to -S_1. \tag{2.72}$$

For operators with definite $R_5^{1,2}$-parity one finds that the associated dimension-5 operators has the opposite $R_5^{1,2}$-parity.

$$\mathcal{O}_0 \to \pm\mathcal{O}_0 \Rightarrow \mathcal{O}_1 \to \mp\mathcal{O}_1. \tag{2.73}$$

Recalling Eq. (2.58), it is easy to show that any even operator under the transformation $R_5^{1,2}$ is automatically $O(a)$-improved since the expected values on the r.h.s are taken with respect to the continuum action. Thus, correlators $f_{X,Y}^{q,r}(x_0, y_0)$ that are even under the transformation $R_5^{1,2}$ are automatically $O(a)$-improved

$$\sum_{\vec{x},\vec{y}} \langle X^{q,r}(x)Y^{r,q}(y)\rangle = \sum_{\vec{x},\vec{y}} \langle X^{q,r}(x)Y^{r,q}(y)\rangle_0 + O(a^2). \tag{2.74}$$

3 SETUP

We present our setup that focuses on controlling the systematic effects for heavy quark physics. We use a mixed-action setup that combines Wilson twisted mass and Wilson fermions on the valence and sea sectors respectively.

We use CLS $N_f = 2 + 1$ ensembles [2] with open boundary conditions in the time direction and periodic boundary conditions in the spatial directions. In section 3.1, we provide details about the sea sector. We use a subset of ensembles listed in Table 3.1 that remains in a chiral trajectory $\mathrm{tr}\, M_{\mathrm{sea}}$. In section 3.3, we explain in more detail the importance of the chiral trajectory.

We employ Wilson twisted mass valence sector with $N_f = 2 + 1 + 1$. We set the valence sector to maximal twist in the light sector, which guarantees automatic $O(a)$ improvement for the desired observables up to residual sea quark mass effects. In section 3.2, we explain the valence regularization.

In section 3.4, we detailed the matching process between the valence and sea sectors in a way that the valence is set at maximal twist. The matching between both sectors is necessary to recover physical results in the continuum limit. We explain the matching for the light and strange dynamical fermions. On the other hand, the charm quark is not present the sea sector. We review different ways to match the charm quark using physical observables.

In section 3.5, we summarize the scale setting procedure [16] performed in our mixed-action setup [17].

3.1 SEA SECTOR

The plaquette action is already $O(a)$-improved, since there are no dimension-5 operators that may contribute to the gauge action. Nevertheless, the $O(a^2)$ effects can be reduced by taking into account dimension-6 operators. There are 3 pure

Id	β	a[fm]	L/a	T/a	M_π[MeV]	M_K[MeV]	$M_\pi L$
H101	3.40	0.087	32	96	420	420	5.8
H102	3.40	0.087	32	96	350	440	4.9
H400	3.46	0.077	32	96	420	420	5.2
N202	3.55	0.065	48	128	420	420	6.5
N203	3.55	0.065	48	128	340	440	5.4
N200	3.55	0.065	48	128	280	460	4.4
N300	3.70	0.050	48	128	420	420	5.1
J303	3.70	0.050	64	196	260	470	4.1

Table 3.1: List of CLS $N_\mathrm{f} = 2+1$ ensembles [2] used in the present study. The values of the inverse bare coupling, $\beta = 6/g_0^2$, correspond to the following approximate values of the lattice spacing [16]. In the fourth and fifth columns, L/a and T/a, refer to the spatial and temporal extent of the lattice. Approximate values of the pion and kaon masses are provided.

gauge dimension-6 operators that can be included. By imposing the equations of motion this leads to the following action

$$S_G = \frac{1}{g_0^2}\sum_{\mu\nu}\left[c_0\sum_p \mathrm{Re}(\mathrm{tr}(1-U_{\mu\nu}(p))) + c_1\sum_r \mathrm{Re}(\mathrm{tr}(1-U_{\mu\nu}(r)))\right], \tag{3.1}$$

where $U_{\mu\nu}(p)$ are the plaquettes and $U_{\mu\nu}(r)$ are planar rectangles. The gauge action used in CLS ensembles is the so-called Lüscher-Weisz action [4], where the values of the coefficients c_0 and c_1 are computed at tree-level

$$c_0 = \frac{5}{3}, \quad c_1 = -\frac{1}{12}. \tag{3.2}$$

The sea sector contains $N_f = 2+1$ dynamical quarks regularized with a non-pertubatively $O(a)$ improved action. We use the standard fermion action introduced in Subsection 2.2.2. The fermionic action contains a dimension-5 operator Eq.

(2.67) that allows to remove $O(a)$ effects according to Symanzik's O(a)-improvement program. To summarize, the fermionic sea action is described by

$$S_F = a^4 \sum_x \bar{\psi}(x) \left[\frac{1}{2}\gamma_\mu(\nabla_\mu + \nabla^*_\mu) + \mathbf{M} - \frac{a}{2}\nabla_\mu\nabla^*_\mu + \frac{ia}{4} c_{\text{sw}} \sigma_{\mu\nu} \mathbf{F}_{\mu\nu} \right] \psi(x), \quad (3.3)$$

where the coefficient c_{sw} is determined non-pertubatively [18].

CLS ensembles [2] use open boundary conditions in the Euclidean time direction over the gauge fields. It has been shown that periodic boundary conditions leads to an increase of the autocorrelations towards the continuum known as critical slowing down [19]. It leads to computationally expensive Monte Carlo simulations to achieve the same target precision. The critical slowing down is related to the existence of disconnected topological sectors [20, 21]. Periodic boundary conditions lead to a disconnected configuration field space towards the continuum. Therefore, the algorithm may not sample different topological sectors.

Open boundary conditions prevent the topological freezing [22, 23] by letting the topological charge to flow through the boundaries. Nevertheless, quark fields are defined with Dirichlet (Schrödinger functional) boundary conditions over Euclidean time. Periodic boundary conditions are imposed over the spatial volume for all the fields.

3.2 VALENCE SECTOR

The valence sector contains $N_f = 2 + 1 + 1$ quark flavors regularized with a Wilson twisted mass action including a clover term [8]. Even though Wilson twisted mass fermions at full twist are automatic $O(a)$-improved, the clover term can be added to the action, which will tweak $O(a^2)$ effects. In addition to this, it has been observed that the clover term reduces isospin breaking effects [24, 25], induced by the regulator. Notice that the valence sector in the chiral limit is equivalent to massless limit with Wilson fermions in the sea. This will allow to recover the renormalization constants from the sea as long as a massless renormalization scheme is used.

We thus use a valence action of the form

$$S_F = a^4 \sum_x \bar{\chi}(x) \left[\frac{1}{2}\gamma_\mu(\nabla_\mu + \nabla^*_\mu) - \frac{a}{2}\nabla_\mu\nabla^*_\mu + \frac{ia}{4} c_{\text{sw}} \sigma_{\mu\nu} \mathbf{F}_{\mu\nu} + \boldsymbol{m}_0 + i\gamma_5 \boldsymbol{\mu} \right] \chi(x), \quad (3.4)$$

where the mass matrix $\boldsymbol{m}_0$ is fixed to the critical mass $\boldsymbol{m}_0 = m_{\rm cr}\mathbb{1}$ and the twisted mass matrix is

$$\boldsymbol{\mu} = \mathrm{diag}(\mu_u, \mu_d, \mu_s, \mu_c) = \mathrm{diag}\left(+|\mu_l|, -|\mu_l|, -|\mu_s|, +|\mu_c|\right). \tag{3.5}$$

The fermion fields $[\chi, \bar{\chi}]$ are expressed in the twisted mass basis. The physical basis is recovered by the following transformation

$$\psi = e^{-i\frac{\pi}{2}\frac{T}{2}\gamma_5}\chi, \quad \bar{\psi} = \bar{\chi}e^{-i\frac{\pi}{2}\frac{T}{2}\gamma_5}, \quad T = \mathrm{diag}(+1, -1, -1, +1). \tag{3.6}$$

Since the heavy doublet is non-degenerate, the twisted valence sector involves a non-traceless component in the chiral rotation, which could contribute to the axial anomaly if this action were used in the sea. This is however not a problem when it is only used in the valence sector, as in this work.

Vector and axial symmetries are broken explicitly in the four flavor theory with non-degenerate quarks. The vector and axial Ward identities can be computed in the twisted basis. For non-diagonal operators, the PCAC and PCVC relations (see Appendix A) are expressed as

$$\partial_\mu A_\mu^{qr} = (m_q + m_r)P^{qr} + i(\mu_q + \mu_r)S^{qr}, \quad (q \neq r), \tag{3.7}$$
$$\partial_\mu V_\mu^{qr} = (m_q - m_r)S^{qr} + i(\mu_q - \mu_r)P^{qr}, \quad (q \neq r). \tag{3.8}$$

The exact vector symmetry for massless fermions guarantee that a point-split current exist $\tilde{V}_\mu^{qr}(x)$ such that the Ward identity Eq. (3.8) remains exact on the lattice.

$$\tilde{V}_\mu^{qr}(x) = \frac{1}{2}\left[\bar{\chi}^q(x)(\gamma_\mu - 1)U_\mu(x)\chi^r(x + a\hat{\mu}) + \bar{\chi}^q(x + a\hat{\mu})(\gamma_\mu + 1)U_\mu^\dagger(x)\chi^r(x)\right],$$
$$\langle \partial_\mu^* \tilde{V}_\mu^{qr}(x)O(0)\rangle = i(\mu_q - \mu_r)\left\langle P^{qr}(x)O(0)\right\rangle. \tag{3.9}$$

The conservation of the Ward identity in the lattice implies that the current $\tilde{V}_\mu^{qr}$ renormalizes with a trivial factor $Z_{\tilde{V}} = 1$, as in the continuum. Therefore, renormalization constants fulfill

$$Z_\mu = Z_P^{-1}, \tag{3.10}$$

where Z_μ and Z_P are the renormalization constants for the twisted mass and the pseudoscalar density respectively.

Applying Symanzik's $O(a)$-improvement program to our mixed action setup [26], we recover automatic $O(a)$-improvement for on-shell quantities at maximal twist

$m_0 = m_{\rm cr}$, whereas valence quark masses get an $O(a)$-contribution from the sea quark masses even at full twist

$$\mu_q^R = Z_\mu(\tilde{g}_0^2, a\mu)\,(1 + a\bar{b}_\mu \mathrm{tr} M_{\rm sea})\,\mu_q, \tag{3.11}$$

where $\tilde{g}_0^2$ is the improved coupling defined as

$$\tilde{g}_0^2 = \left(1 + a\frac{b_g}{3}\mathrm{tr}\, M_{\rm sea}\right) g_0^2. \tag{3.12}$$

The effects of this contribution are expected to be of order $\bar{b}_\mu = O(g_0^4)$ in perturbation theory and therefore the term is expected to be negligible for lattice spacings $a \lesssim 0.086\,\mathrm{fm}$ and light/strange quark masses in $M_{\rm sea}$.

The valence sector can be regularized with Osterwalder-Seiler fermions [15, 27] in a similar way. This framework allows to simplify computation and renormalization of complex composite operators.

3.3 CHIRAL TRAJECTORY

We perform our computations on a set of CLS ensembles with different values of the lattice spacing in the range $0.05\,\mathrm{fm} \lesssim a \lesssim 0.087\,\mathrm{fm}$ and pion masses that vary in the range $260\,\mathrm{MeV} \lesssim M_\pi \lesssim 420\,\mathrm{MeV}$. In order to extract physical results at the physical point, we choose a chiral trajectory where the trace of the bare mass matrix is kept constant $\mathrm{tr}\, M_{\rm sea} = \mathrm{const}$. The main advantage of this trajectory is that the improved coupling Eq. (3.12) is constant at fixed value of the bare coupling g_0^2, and therefore so is the renormalized coupling $g_R^2 = Z_g g_0^2$ up to $O(a^2)$ effects. In practice, the condition is not easy to satisfy since it contains the subtracted masses. It has been reported [16] that deviations from the renormalized chiral trajectory are not negligible, meaning that simulations are not on a line of constant physics.

Actually, we redefine the chiral trajectory in terms of the pseudoscalar meson masses, that coincide with the renormalized values of the quark masses in chiral perturbation theory at leading order. This choice turns out to be more beneficial, since pseudoscalar masses do not rely on renormalization constants or $O(a)$-improvement coefficients. We choose a line of constant physics, where the quantity ϕ_4 is kept constant

$$\phi_4 = 8t_0\left(M_K^2 + \frac{1}{2}M_\pi^2\right) \propto \mathrm{tr}\, M_{\rm sea}^R, \tag{3.13}$$

where t_0 is the gradient flow reference scale (see Subsection 4.3.1). Deviations from the renormalized chiral trajectory can be corrected at the level of analysis by performing a Taylor expansion on the quark masses [16]. The values of ϕ_4 for each ensemble are shifted to compensate the mistuning.

For a general observable $F = f(P_i)$ that depends on several primary observables P_i, the Taylor expansion at linear order reads

$$F'(m_l', m_s') = F(m_l, m_s) + 2\Delta m_l \frac{\mathrm{d}F(m_l, m_s)}{\mathrm{d}m_l} + \Delta m_s \frac{\mathrm{d}F(m_l, m_s)}{\mathrm{d}m_s}, \tag{3.14}$$

where the total derivative with respect to the quark masses takes the form

$$\frac{\mathrm{d}F}{\mathrm{d}m_f} = \sum_i \frac{\partial F}{\partial \overline{P}_i} \left[\left\langle \frac{\partial P_i}{\partial m_f} \right\rangle - \left\langle \left(P_i - \overline{P}_i\right) \left(\frac{\partial S}{\partial m_f} - \frac{\overline{\partial S}}{\partial m_f} \right) \right\rangle \right]. \tag{3.15}$$

We choose a line towards the renormalized chiral trajectory such that $\Delta m_l = \Delta m_s$. This fixes all the remaining degrees of freedom in the procedure.

The derivative receives contributions from the valence and sea quarks respectively. The first term in the r.h.s. of the equation is related to the valence contribution and in a unitary setup it corresponds to derivative of a two-point function with respect to the sea mass. In practice, this term implies the computation of additional inversions of the Dirac operator for each two-point function.

$$\begin{aligned} &\frac{\partial}{\partial m_f} \langle \bar{q}^r(x) \Gamma_X q^s(x) \bar{q}^s(y) \Gamma_Y q^r(y) \rangle \\ &= -\delta_{f,s} \mathrm{tr} \left[\Gamma_X (D + m_s)^{-2}(x,y) \Gamma_Y (D + m_r)^{-1}(y,x) \right] \\ &\quad -\delta_{f,r} \mathrm{tr} \left[\Gamma_X (D + m_s)^{-1}(x,y) \Gamma_Y (D + m_r)^{-2}(y,x) \right]. \end{aligned} \tag{3.16}$$

The sea contribution requires the computation of the derivative of the action with respect to the sea quark masses, which is given by the trace of the propagator

$$\frac{\partial S}{\partial m_f} = -\mathrm{tr} \left[(D + m_f)^{-1} \right]. \tag{3.17}$$

The strategy to compute shifted observables is the following:

1. We compute ϕ_4 in the unitary Wilson setup.

2. We determine the value of the mass shift $\Delta m = \Delta m_l = \Delta m_s$ such that ϕ_4 is shifted to some physical value ϕ_4^{phys}.

3. We compute the desired observables in our mixed-action setup for each ensemble.

4. We shift the observables to the renormalized chiral trajectory, where $m_f \to m_f + \Delta m$.

Notice that valence observables computed in out mixed-action setup do not depend explicitly on the sea masses m_f. Therefore, the first term on the r.h.s. of Eq. (3.15) does not contribute to the final result.

3.4 MATCHING

In order to obtain controlled results for the valence sector, we need to ensure that physical obervables computed in the valence and sea sectors coincide up to cutoff effects, *i.e.* coincide in the continuum limit. Therefore, a well-defined matching procedure is required at finite lattice spacing.

In general, once the lattice spacing is fixed, typically in terms of some reference scale, *e.g.* , t_0, two matching conditions are needed for the light and strange quark masses. Naively, the matching condition is to impose that the renormalized quarks masses are the same for the valence and sea sectors $m_q^R\big|_{\text{sea}} = \mu_q^R\big|_{\text{val}}$. Nevertheless, other choices are possible, *e.g.* , imposing that pion and kaon masses are the same in the two sectors. We studied both matching conditions in our setup, and we performed consistency checks for both matching conditions [28]. We chose the matching through meson masses as our preferred matching condition because it does not require $O(a)$ counterterms.

We will describe the matching procedure through pseudoscalar meson masses. In order to perform this matching, the mass matrix $\boldsymbol{m}_0$ is tuned to its critical value $\boldsymbol{m}_0 = m_{\text{cr}}\mathbb{1}$ and the bare twisted masses μ_l and μ_s to some values that satisfy the matching condition

$$\phi_2|_{\text{sea}} = \phi_2|_{\text{val}}\,, \quad \phi_4|_{\text{sea}} = \phi_4|_{\text{val}}\,, \tag{3.18}$$

where the variables ϕ_2 and ϕ_4 are the following mass combinations:

$$\phi_2 = 8t_0 M_\pi^2, \quad \phi_4 = 8t_0\left(M_K^2 + \frac{1}{2}M_\pi^2\right). \tag{3.19}$$

We use PCAC masses in our Wtm valence sector to fix the renormalized twist angle at maximal twist ($\omega_R = \pi/2$). PCAC masses are defined by the Ward identities in Eq. (3.7). We compute the PCAC mass for the light sector as follows

$$m_{ll} \equiv \frac{m_u + m_d}{2} = \frac{\langle \partial_\mu A_\mu^{ud}(x) P^{ud}(y) \rangle}{2 \langle P^{ud}(x) P^{ud}(y) \rangle}, \tag{3.20}$$

where the expression is simplified in our valence setup provided that $\mu_u = -\mu_d$. The PCAC mass m_{ll} is a measure of the bare quark mass. Therefore, the point with a vanishing value of the PCAC mass correspond to the maximal twist case.

The strategy requires the computation of two-point functions on a three dimensional grid of parameters (m, μ_l, μ_s) for each ensemble. We perform combined interpolations to a target point that fulfills the matching conditions and ensures that the setup is at maximal twist.

From the definition of polar mass Eq. (2.28), we compute the renormalized quark mass $M_q^R\big|_{\text{val}}$ and then perform a Taylor expansion assuming that m is close to its critical value neglecting any

$$M_q^R\big|_{\text{val}} = \sqrt{(Z_\mu \mu_q)^2 + (Z_m (m - m_{\text{cr}}))^2} \simeq Z_\mu \mu_q + \frac{Z_M^2}{2 Z_\mu \mu_q} (m - m_{\text{cr}})^2. \tag{3.21}$$

We take advantage of chiral perturbation theory at tree level to parametrize the meson masses in terms of the bare parameters.

$$M_\pi^2\big|_{\text{val}} \simeq 2B\, M_l^R\big|_{\text{val}} \simeq 2B Z_\mu \mu_l + B \frac{Z_m^2}{Z_\mu \mu_l} (m - m_{\text{cr}})^2, \tag{3.22}$$

$$\begin{aligned} M_K^2\big|_{\text{val}} &\simeq B \left(M_l^R\big|_{\text{val}} + M_s^R\big|_{\text{val}} \right) \\ &\simeq B Z_\mu (\mu_l + \mu_s) + B \frac{Z_m^2}{2 Z_\mu} \left(\frac{(m - m_{\text{cr}})^2}{\mu_l} + \frac{(m - m_{\text{cr}})^2}{\mu_s} \right). \end{aligned} \tag{3.23}$$

Assuming that the values of the twisted mass μ_l are constant when varying the values of m close to its critical value. We perform a combined fit over the PCAC mass $m_{ll}|_{\text{val}}$ (Eq. 3.20) and the variables (ϕ_2, ϕ_4) with the following functional form

$$m_{ll}|_{\text{val}}\,(\mu_l,\, m) = c_0^1 + c_1^1 \mu_l + c_2^1 m \equiv 0, \tag{3.24}$$

$$\phi_2|_{\text{val}}\,(\mu_l,\, m) = c_0^2 + c_1^2 \mu_l + c_2^2 m + c_3^2 m^2 \equiv \phi_2|_{\text{sea}}\,, \tag{3.25}$$

$$\phi_4|_{\text{val}}\,(\mu_l,\, \mu_s,\, m) = c_0^3 + c_1^3 \mu_l + c_2^3 \mu_s + c_3^3 m + c_4^3 m^2 \equiv \phi_4|_{\text{sea}}\,. \tag{3.26}$$

The values $\phi_2|_{\text{sea}}$ and $\phi_4|_{\text{sea}}$ correspond the values of ϕ_2 and ϕ_4 on the renormalized chiral trajectory.

3.4.1 Charm sector

The matching procedure for the charm sector requires a different strategy, since in our setup the charm is not a dynamical fermion. In order to establish a connection with physics, we require that some charm observable $\mathcal{O}_c$ is equal to its physical value on each ensemble. The matching condition ensures the correct limit once chiral and continuum extrapolations are performed.

We studied three different matching conditions based on a spin-flavor-averaged and flavor-averaged mass combinations of mesons masses and on the connected contribution of the η_c mass.

$$M_c^{\text{f}} = \frac{1}{3}\left(2M_D + M_{D_s}\right), \tag{3.27}$$

$$M_c^{\text{s-f}} = \frac{1}{12}\left(2M_D + M_{D_s} + 6M_{D^*} + 3M_{D_s^*}\right), \tag{3.28}$$

$$M_c^{\eta} = M_{\eta_c^{(\text{conn})}}. \tag{3.29}$$

The matching can be performed by introducing the three matching conditions ϕ_c^i in terms the reference scale t_0 and then interpolate them to their physical values for each ensemble.

$$\begin{aligned} \phi_{c,1} &= \sqrt{8t_0} M_c^{\text{f}} \equiv \sqrt{8t_0^{\text{phys}}} (M_c^{\text{f}})^{\text{phys}}, \\ \phi_{c,2} &= \sqrt{8t_0} M_c^{\text{s-f}} \equiv \sqrt{8t_0^{\text{phys}}} (M_c^{\text{s-f}})^{\text{phys}}, \\ \phi_{c,3} &= \sqrt{8t_0} M_c^{\eta} \equiv \sqrt{8t_0^{\text{phys}}} M_{\eta_c}^{\text{phys}}. \end{aligned} \tag{3.30}$$

However, this method includes some complications. The meson masses in each ensembles are not computed at the physical value of ϕ_2 and contains $O(a^2)$ effects but they are matched to their physical value. Moreover, it introduces the dependence on the the physical scale t_0^{phys} for charmed observables at finite lattice spacing. For these reasons, we prefer to perform the charm quark matching in the continuum and chiral extrapolation. We parametrize the dependence of a given observable $\mathcal{O}_c(a^2,\, \phi_2,\, \phi_c)$ on the charm quark mass and perform a combined fit to its physical value $\mathcal{O}_c(0,\, \phi_2|_{\text{phys}},\, \phi_c|_{\text{phys}})$. In our study, we use the three matching conditions $\phi_{c,i}$. In chapter 5, we will describe the functional forms for the chiral and continuum extrapolations.

3.5 SCALE SETTING

In this section we review the scale setting procedure in our setup. We follow the strategy proposed by [16] to determine the physical value of the reference scale $t_0^{\rm phys}$. We have reproduced the results for the scale setting in our setup [17, 29], where different matching conditions in the light sector are imposed.

The physical value of t_0 cannot be measured by experiments, although it can be determined in lattice simulations. The physical values of the pion and kaon decay constants and masses are used as input for the determination of the reference scale. The linear combination of decay constants

$$f_{\pi K} = \frac{2}{3}\left(f_K + \frac{1}{2}f_\pi\right), \tag{3.31}$$

is advantageous following the chiral trajectory $\mathrm{tr}M = \text{const.}$. It shows a mild dependence in the meson masses through chiral logarithms at NLO in chiral perturbation theory. The physical point $(\phi_2^{\rm phys}, \phi_4^{\rm phys})$ depends on the physical value of the reference scale and it is determined using a iterative algorithm that stops when the algorithm provide compatible values of $t_0^{\rm phys}$ within errors. The procedure starts with an initial value of $t_0^{{\rm phys},k}$, which defines physical point at the k-th iteration $(\phi_2^{{\rm phys},k}, \phi_4^{{\rm phys},k})$. The algorithm consist in:

1. The values of $\phi_2^{{\rm phys},k}$ and $\phi_4^{{\rm phys},k}$ are computed using the physical values of the pion and kaon mass

$$\begin{aligned} \phi_4^{{\rm phys},k} &= 8t_0^{{\rm phys},k}((M_K^2)^{\rm phys} + \frac{1}{2}(M_\pi^2)^{\rm phys}), \\ \phi_2^{{\rm phys},k} &= 8t_0^{{\rm phys},k}(M_\pi^2)^{\rm phys}. \end{aligned} \tag{3.32}$$

2. The values of $f_{\pi K}$ are computed for each ensemble. Then, the observables are shifted to the new value $\phi_4^{{\rm phys},k}$ that defines the chiral trajectory (see Section 3.3).

3. A functional form for $\sqrt{8t_0}f_{\pi K}(a, \phi_2)$ is chosen to extrapolate the results in the continuum limit and physical point.

4. The extrapolated value of $f_{\pi K}$ defines the value $(k+1)$-th iteration

$$\sqrt{8t_0^{{\rm phys},k+1}}\, f_{\pi K}^{\rm phys} \equiv \sqrt{8t_0} f_{\pi K}\left(0,\, \phi_2^{{\rm phys},k}\right). \tag{3.33}$$

We quote the results from [17] that combines the results from the unitary Wilson setup and our mixed-action setup with two different matching conditions.

$$t_0^{\text{phys}} = 0.02140(26)(27)\,\text{fm}^2, \qquad \phi_4^{\text{phys}} = 1.114(14)(14). \tag{3.34}$$

4 COMPUTATION OF OBSERVABLES

In this chapter we review the main algorithms that are involved in our work. In section 4.1, we briefly review how the Hybrid Monte Carlo [30] algorithm works on Lattice QCD simulations. In section 4.2, we explain how the two-point functions are computed in the simulation. We also review the Distance Preconditioning [31] technique that is of crucial relevance to obtain heavy propagators precisely.

In section 4.3, we detail the methods to determine the physical observables that will be used in our study. We describe the computation of fermionic observables such that: meson masses, quark masses, and pseudoscalar decay constants. We also introduce the reference scale t_0 [32] that will be used to extract results in physical units.

4.1 MONTE CARLO ALGORITHM

Computation of observables in Lattice QCD is performed by determining expectation values using the Lagrangian formalism. Lattice QCD relies on Markov Chain Monte Carlo action methods to estimate a path integral. In Euclidean space, the action can be interpreted as a probability distribution function $P(U) = e^{-S_G[U]-S_{\text{eff}}[U]}$ (see Section 2.3). Therefore, the result of the integral can be approximated by sampling the configuration space numerically,

$$\langle \mathcal{O} \rangle = \frac{1}{Z} \int \mathcal{D}[U]\, \mathcal{O}[U] P(U) = \frac{1}{N} \sum_{i=1}^{N} \mathcal{O}[U_i] + O\left(\frac{1}{\sqrt{N}}\right), \tag{4.1}$$

where $\mathcal{O}[U_i]$ are generated given the probability distribution function $P(U)$. The statistical error is expected to decrease with the square root of the number of samples N, as indicated.

4.1.1 Hybrid Monte Carlo

The simulation with dynamical fermions increases the difficulty of the sampling. The fermion determinant (Eq. (2.34)) is a non-local term on the gauge links. Therefore,

sampling Wilson links locally becomes costly and proportional to the volume squared. The Hybrid Monte Carlo (HMC) algorithm [30] updates the Wilson links globally. HMC algorithm takes advantage of the Hamiltonian formalism to generate a proposal with high acceptance rate. This is performed by augmenting the field space with the canonical conjugate fields $\pi_\mu(x)$. Then, the equations of motion are solved according to the Hamilton-Jacobi equation at a given Monte Carlo time τ. In this new formalism the probability of each trajectory is given by the Hamiltonian. We extend the partition function $\mathcal{Z}$ with the conjugate fields $\pi_\mu(x)$

$$\begin{aligned} \mathcal{Z} &= \int \mathcal{D}U\mathcal{D}\pi\, e^{-H[\pi,U]}, \\ H &= \sum_x \frac{1}{2}\mathrm{tr}\{\pi_\mu^\dagger(x)\pi_\mu(x)\} + S_G[U] + S_{\text{eff}}[U], \end{aligned} \tag{4.2}$$

where the fields $\pi_\mu(x)$ are element of the Lie algebra. Notice that expectation values of observables remain unchanged because integration over the conjugate fields leads to a normalization factor

$$\begin{aligned} \langle \mathcal{O}(x_1,\dots,x_n)\rangle &= \frac{1}{\mathcal{Z}}\int \mathcal{D}U\mathcal{D}\pi\, \mathcal{O}(x_1,\dots,x_n)e^{-H[\pi,U]} \\ &= \frac{1}{Z}\int \mathcal{D}U\, \mathcal{O}(x_1,\dots,x_n)e^{-S_G[U]-S_{\text{eff}}[U]}, \end{aligned} \tag{4.3}$$

where Z is the usual partition function defined in Eq. (2.36).

The equations of motion of the fields with respect to the Monte Carlo time τ are the following

$$\frac{\mathrm{d}U_\mu(x)}{\mathrm{d}\tau} = \pi_\mu(x)U_\mu(x), \tag{4.4}$$

$$\frac{\mathrm{d}\pi_\mu(x)}{\mathrm{d}\tau} = -F_\mu(x) = -\frac{\mathrm{d}S}{\mathrm{d}U_\mu}, \tag{4.5}$$

where the derivative of a scalar function with respect to a group element is defined in [33].

$$\frac{\mathrm{d}S}{\mathrm{d}U_\mu} = \left.\frac{\mathrm{d}S(e^\omega U)}{\mathrm{d}\omega}\right|_{\omega=0}, \quad \omega \in \mathfrak{su}(N). \tag{4.6}$$

The integration of the equations of motion provides a proposal for the configuration with a high acceptance ratio. The algorithm consists in:

1. generate canonical momentum variables $\pi_\mu(x)$ according to a standard normal distribution

$$\pi_\mu(x) \sim \mathcal{N}(0,1). \tag{4.7}$$

2. integrate the Hamilton equations numerically to compute the updated canonical variables $(\pi, U) \to (\pi', U')$. Numerical integration is carried out through a discretization with a determined number of integration steps such that the trajectory length is fixed.

3. the proposal is accepted according to the following acceptance probability:

$$P_{\text{acc}} = \min(1, e^{-(H(\pi',U')-H(\pi,U))}). \tag{4.8}$$

   The configuration is stored if $P_{\text{acc}} > r$, where r is a random uniformly distributed random variable and $0 \leq r < 1$.

Since the Hamiltonian is conserved the acceptance ratio will be $P_{\text{acc}} = 1$ if the equations are exactly solved. In practice, the acceptance ratio is high because the Hamiltonian is conserved up to integration errors. It is important to mention that a reversible solver for the equations of motions is required since molecular dynamics are time reversible.

Modern HMC simulations include several performance improvements. Efficiency can be improved using a multiple time-step integrator [34] and an improved integrators such as the one proposed by Omelyan, Mryglod and Folk [35]. Other improvements related with the fermion determinant can be implemented, as discussed below.

4.1.2 Reweighting

As a consequence of the chiral symmetry breaking in the lattice, the Wilson-Dirac operator is not protected against zero eigenvalues. These zero modes may lead to some instabilities [7] in the Hybrid Monte Carlo. In order to avoid this problem, the computation of the fermion determinant is factorized by separating the low-energy modes.

In CLS configurations [2], the light quark determinant is shifted with a twisted mass term [36] that provides an infrared cutoff similarly to the determinant for twisted mass fermions Eq. (2.39). On the other hand, the strange quark determinant is computed using a rational approximation [37, 38].

For the light and strange quarks, the contributions are factorized in terms of the reweighting factors W_l and W_s respectively.

$$\det(D_l^\dagger D_l) = \det(\tilde{D}_l^\dagger \tilde{D}_l) W_l, \tag{4.9}$$

$$\det(D_s) = \frac{P_1(D_s^\dagger D_s, n)}{P_2(D_s^\dagger D_s, n)} W_s, \tag{4.10}$$

where $\tilde{D}_l$ is a Dirac operator with a twisted mass term and $P_{1,2}(D_s^\dagger D_s, n)$ are polynomials of degree n such that $\frac{P_1(D_s^\dagger D_s,n)}{P_2(D_s^\dagger D_s,n)} \approx \det\left(\sqrt{D_s^\dagger D_s}\right)$.

Therefore, in order to recover physical results with respect to the actual action, expectation values of operators are redefined as follows

$$\langle \mathcal{O} \rangle_{\text{rew}} = \frac{\langle \mathcal{O} W_l W_s \rangle}{\langle W_l W_s \rangle}. \tag{4.11}$$

There are different parameterizations for the twisted mass reweighting. We present the current parametrization in CLS ensembles [2].

$$\det(\tilde{D}^\dagger \tilde{D}) = \frac{\det(D^\dagger D + \mu^2)^2}{\det(D^\dagger D + 2\mu^2)}, \quad W_l = \det(D^\dagger D)\frac{\det(D^\dagger D + 2\mu^2)}{\det(D^\dagger D + \mu^2)^2}. \tag{4.12}$$

The reweighting can be complemented using the Hasenbusch factorization [39, 40] to improve the computation of the determinants. The even-odd preconditioning [41] for the Dirac operator can be added as well.

4.2 INVERSIONS

In order to measure fermionic observables, inversions of the Dirac operator resulting from Wick contractions are required. In this section, we sketch out how the inversions are computed without going through the algorithmic details. We define a general two-point function $f^{q,r}(x_0, y_0)$ and work out the Wick contractions:

$$\begin{aligned} f^{q,r}(x_0, y_0) &= \frac{1}{L^3} \sum_{\vec{x},\vec{y}} \left\langle \bar{\psi}_q(x) \Gamma_A \psi_r(x) \bar{\psi}_r(y) \Gamma_B \psi_q(y) \right\rangle, \\ f^{q,r}(x_0, y_0) &= -\frac{1}{L^3} \sum_{\vec{x},\vec{y}} \left\langle \mathrm{tr}\{\Gamma_A D_r^{-1}(x,y) \Gamma_B D_q^{-1}(y,x)\} \right\rangle, \end{aligned} \tag{4.13}$$

where the indices q, r denote flavor, $\Gamma_{A,B}$ are some spin matrices, and color and spin indices are traced over. The computation of correlators requires the inversion of Dirac operators. The all-to-all computations of those inversions,

$$D_q(x,y)\psi_r(y) = \delta_{x,y}\,\delta_{q,r}, \tag{4.14}$$

can be computationally too expensive for practical lattices. The stochastic procedure allows to estimate the inversions given a set of stochastic sources. A set of stochastic fermionic fields $[\eta]_i$ $(i = 1, \ldots, N_\eta)$ are introduced such that they fulfill:

$$\langle \eta_i(x) \rangle_\eta = 0, \qquad \left\langle \eta_j(y)^\dagger \eta_i(x) \right\rangle_\eta = \delta_{x,y}\, \delta_{i,j}. \tag{4.15}$$

The expectation value $\langle \cdot \rangle_\eta$ is defined with a given noise distribution for the stochastic sources. Some common choices for that are Gaussian, Z_2 or $U(1)$ distributions. We define two derived stochastic quantities by inverting the Dirac operators D_q and D_r with a given stochastic source.

$$\begin{aligned} \zeta_i^q(x) &= \sum_y D_q^{-1}(x,y)\eta_i(y), \\ \xi_i^r(x) &= \sum_y D_r^{-1}(x,y)\gamma_5 \Gamma_A^\dagger \eta_i(y). \end{aligned} \tag{4.16}$$

Notice that for the pion case, only one inversion is required for that since both stochastic vectors are identical. Therefore, Eq. (4.15) guarantees that the correlator $f^{q,r}(x_0, y_0)$ can be computed as follows

$$f^{q,r}(x_0, y_0) = -\frac{1}{L^3} \sum_{\vec{x}} \left\langle \left\langle \left(\Gamma_B^\dagger \gamma_5 \xi_i^r(x) \right)^\dagger \zeta_i^q(x) \right\rangle_\eta \right\rangle. \tag{4.17}$$

Solving the Dirac equations for a sufficiently large set of stochastic sources gives a precise estimate of the solution. In practice, the correlator $f^{q,r}(x_0, y_0)$ can be estimated as

$$f^{q,r}(x_0, y_0) \approx -\frac{1}{L^3} \frac{1}{N_\eta} \sum_{i=1}^{N_\eta} \sum_{\vec{x}} \left\langle \left(\Gamma_B^\dagger \gamma_5 \xi_i^r(x) \right)^\dagger \zeta_i^q(x) \right\rangle. \tag{4.18}$$

Moreover, we take advantage of spin dilution [42,43] in order to get variance reduction for charm-like observables. Stochastic sources are projected into spin subspace $\eta_i^a(x) = P^a \eta_i(x)$.

$$\begin{aligned} \zeta_i^{q,a}(x) &= \sum_y D_q^{-1}(x,y)\eta_i^a(y), \\ \xi_i^{r,a}(x) &= \sum_y D_r^{-1}(x,y)\gamma_5 \Gamma_A^\dagger \eta_i^a(y), \\ f^{q,r}(x_0, y_0) &\approx -\frac{1}{L^3} \frac{1}{N_\eta} \sum_{i=1}^{N_\eta} \sum_a \sum_{\vec{x}} \left\langle \left(\Gamma_B^\dagger \gamma_5 \xi_i^{r,a}(x) \right)^\dagger \zeta_i^{q,a}(x) \right\rangle. \end{aligned} \tag{4.19}$$

Notice that $\xi_i^{r,a}(x)$ can be rewritten in terms of a linear combinations of the projections for each gamma structure Γ_A. Therefore, by inverting the full set of projections $\eta_i^a(x)$ the full set of independent gamma structures can be computed by performing Wick contractions, at the price of four inversions for each propagator.

4.2.1 Distance preconditioning

Numerical inversions of the Dirac operator may introduce technical difficulties when inverting heavy masses. Numerical algorithms find a solution to the inhomogeneous Dirac operator (Eq. (3.4)) such that it fulfills the condition

$$\left|(D_q[U](x,y))S_q^n(x) - \eta(y)\right| < r, \tag{4.20}$$

where $S_q^n(x)$ is the approximate solution after n solver iterations and $\eta(y)$ is the noise vector, previously introduced. The global residue r fixes the target precision of the current inversion.

As a result of Eq. (2.50), two-point correlation functions decay as $e^{-M(x_0-y_0)}$, where M stands for the mass of the ground state. The exponential behavior of this function may provide a negligible contribution to the norm of on the l.h.s of Eq. (4.20). This issue may introduce problems in the propagator accuracy at large time extents. Hence, it may lead to noisy solutions at large distances that are not useful for the extraction of physical results. The problem is aggravated when dealing with heavy propagators due to the fast exponential decay.

Distance preconditioning [31] is a technique that improves the inversion accuracy. The system is transformed by adding an exponential factor that partially compensates for the fast decay of the propagator. Then, the system is solved and the transformation is reverted.

We introduce a diagonal matrix in Euclidean space P as follows,

$$P = \mathrm{diag}(p_1, p_2, \ldots, p_T), \qquad p_i = e^{\alpha\left|x_0^i - y_0\right|}, \tag{4.21}$$

where the parameter α controls the suppression of the exponential decay. The Dirac operator and the noise vector are then transformed as

$$\begin{aligned} D' = PDP^{-1}, \qquad \eta' = P\eta, \\ D'(x,y)S'(x) = \eta'(y), \end{aligned} \tag{4.22}$$

where S' is the preconditioned propagator $S' = PS$. Then, S' is computed by solving the preconditioned system (Eq. (4.22)). The actual propagator S is computed by reversing the transformation with P^{-1}.

The distance preconditioning increases the cost of the inversions roughly proportionally to the value of the α parameter. In our study, we tune the α parameter for each ensemble such that it is large enough to avoid the deterioration of the signal at large Euclidean times, while the cost increase is under control. In order to do that, at fixed global residue r and the source position y_0, we compute mass-degenerate pseudoscalar-pseudoscalar correlators from preconditioned propagators with different values of α. We choose the minimal value of α that guarantees a clear signal in the correlator at large distances. This tuning is performed with low-statistics runs for each ensemble. In figure 4.1 we show a example in a particular CLS ensemble using propagators around the charm quark mass region.

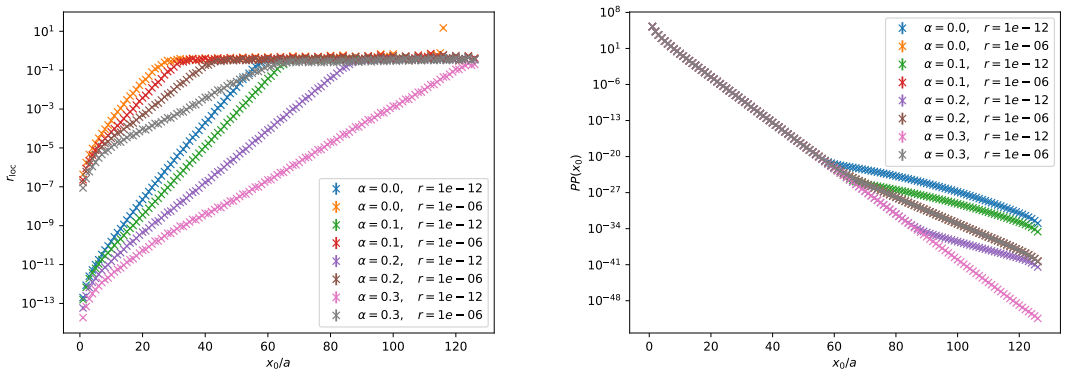

Figure 4.1: Values of the average local residue r_{loc} and pseudoscalar-pseudoscalar correlation function $PP(x_0)$ as a function of the Euclidean time x_0/a. The two-point correspond to a mass degenerate meson with twisted mass $a\mu = 0.2$. The inversions are performed on a 128×48^3 lattice and the source position is fixed close to the left boundary. Different colors represent different combinations of the global residue r and α parameter.

4.3 OBSERVABLES

In this section, we detail the computation of physical observables on the lattice that we will use in our study. We also introduce the gluonic observable t_0 that we use as a reference scale.

Meson masses and decay constants are extracted from two-point correlation functions. We recall our convention for the correlators

$$f^{q,r}_{X,Y}(x_0, y_0) = \frac{a^6}{L^3} \sum_{\vec{x},\vec{y}} \langle X^{q,r}(x) Y^{r,q}(y) \rangle \,, \tag{4.23}$$

where q and r are flavor indices. X and Y represent different Dirac bilinears (see Appendix A). We use stochastic spin-diluted sources defined at a given time slice in the middle of the lattice ($y_0 = T/2$) in order to avoid operator couplings to boundary states, induced by the use of non-periodic boundary conditions in time. We use the $U(1)$ noise distribution to estimate the propagators. The Distance Preconditioning technique is used for propagators with masses in the charm region as detailed in Subsection 4.2.1.

Our mixed-action setup requires additional computations of correlators in the unitary setup. These correlators are used to match the sea and the valence sectors for the mixed-action setup and therefore recover unitarity in the continuum limit. Moreover, the computation of those correlators is crucial in order to compute the mass corrections to the renormalized chiral trajectory. The procedures are detailed in Sections 3.4 and 3.3. Notice that valence (Wtm) correlators may be expressed in the physical or twisted basis. The change of basis is detailed in Appendix B.

In our setup, the quark masses can be measured from the twisted mass parameter μ_q. We will describe the determination of renormalization group invariant (RGI) quark masses from the values of the twisted mass.

4.3.1 Gradient flow scale t_0

The gradient flow formalism [32, 44] allows to smooth gauge fields in a field-theoretically well-controlled way, as a result of which ultraviolet divergences can be avoided. The gradient flow can be used to define observables that are useful for scale setting, study of the topological susceptibility, or computing the running couplings, among other examples. The gauge fields are extended to a 5-dimensional theory with the flow time t as an extra spacetime dimension. The gauge fields fulfill the flow equation

$$a^2 \frac{\mathrm{d}V_\mu}{\mathrm{d}t}(x,t) = -g_0^2 \frac{\delta S[V]}{\delta V_\mu(x,t)} V_\mu(x,t), \quad V_\mu(x,t=0) = U_\mu(x), \tag{4.24}$$

where $V_\mu(x,t)$ are the Wilson links extended to the 5-dimensional theory. The flow time t can be interpreted in terms of the average radius of a 4-dimensional sphere where the short distance fluctuations are averaged within $r \approx \sqrt{8t}$. This is easily shown by solving the flow equations at leading order for the gauge fields $B_\mu(x,t)$ and $A_\mu(x)$

$$B_\mu(x,t) = \frac{1}{(4\pi t)^2} \int \mathrm{d}^4 y \, e^{\frac{(x-y)^2}{4t}} A_\mu(y). \tag{4.25}$$

By taking the limit $t \to \infty$ the classical theory is recovered. The action density is a finite quantity at non-vanishing flow time and does not require renormalization [45],

$$\langle E(x_0,t)\rangle = \frac{1}{4}\sum_{\boldsymbol{x}} \langle \mathrm{tr}\left(G_{\mu\nu}(x,t)G_{\mu\nu}(x,t)\right)\rangle\,, \tag{4.26}$$

where $G_{\mu\nu}(x,t)$ is the field strength tensor in the 5d theory. According to perturbation theory, the energy density $E(x_0,t)$ scales towards the continuum as a dimension 4 observable. Following [32], se use the following expression to define the reference scale t_0

$$\left\langle \langle t^2 E(x_0,t)\rangle_{x_0} \right\rangle\Big|_{t=t_0} = 0.3. \tag{4.27}$$

The value on the r.h.s of the equation is chosen because the behavior in that region is very approximately linear with respect to the flow time t, and data points within that region have low statistical errors.

First of all, we fit the energy density $E(x_0,t)$ over plateaux in Euclidean time for each value of the flow time, *i.e.* we apply a weighted average in the plateau region.

$$E(t) = \langle E(x_0,t)\rangle_{x_0}\,. \tag{4.28}$$

Then, we perform a polynomial fit of the quantity $\langle t^2 E(t)\rangle$ in the region where $\langle t^2 E(t)\rangle \approx 0.3$. As we have mentioned before, the behavior in that region is very approximately linear. We use a linear fit as our preferred functional form. Once the fit is performed, we find the value of the flow time t that fulfills Eq. (4.27).

The energy density definition depends on the regularization of the field strength tensor. We choose the Wilson plaquette action for that purpose.

$$E(x_0,t) = 2\sum_{\vec{x}} \mathrm{tr}\{1 - V_{\mu\nu}(x,t)\}. \tag{4.29}$$

The physical value of the reference scale t_0 has been computed for CLS ensembles in [16, 17].

4.3.2 Meson masses

In our setup, the meson masses are used for computing the renormalized chiral trajectory and matching the quark masses to some target value. For the light and strange quarks, we use the pseudoscalar meson masses M_π and M_K to match the sea and valence sectors, whereas for the charm quark (quenched), we use different combinations of meson masses to match them to some physical quantity (see Sections 3.3 and 3.4).

The ground state meson masses are easily obtained by observing two-point functions at large time extents in the bulk, where the exponential decay is dominated by the lowest energy state (see Eq. (2.50)).

In practice, the meson masses are computed through the effective mass that is defined as follows

$$aM_{qr}^{\text{eff}}(x_0) = \ln\left|\frac{f^{q,r}(x_0,y_0)}{f^{q,r}(x_0+1,y_0)}\right|, \tag{4.30}$$

where the operator indices are implicit. The effective mass cancels the normalization of two-point correlation functions and it provides a plateau in the region where the decay is dominated by the ground state. The actual value of the meson mass is computed by fitting the effective mass function to a plateau neglecting correlations between different time slices in the plateau region.

Correlators $f^{q,r}_{\mathcal{P}\mathcal{P}}$ and $f^{q,r}_{\mathcal{V}_i\mathcal{V}_i}$ provide information for the pseudoscalar meson masses and vector meson masses, respectively. Charmed vector meson masses are used in the spin-flavor averaged mass combination Eq. (3.28) as one of our matching conditions for the charm quark mass.

4.3.3 Quark masses

Renormalized quark masses are easily determined at maximal twist since there is no additive renormalization terms to the mass and the twisted mass μ_q is a parameter in our computations. As discussed in Section 3.2, renormalized twisted mass takes the form

$$\mu_q^R = Z_\mu(g_0^2, a\mu)\mu_q, \quad Z_\mu(g_0^2, a\mu) = Z_P^{-1}(g_0^2, a\mu), \tag{4.31}$$

where μ_q^R is $O(a)$-improved up to $O(a\text{tr}\, M_{\text{sea}})$ effects that are expected to be negligible in our current setup.

We use the results from [46] to compute the renormalization group invariant (RGI) quark masses at $N_f = 3$,

$$m_q^{\text{RGI}} = Z_M^{\text{tm}}(g_0^2)\mu_q. \tag{4.32}$$

The factor $Z_M^{\text{tm}}(g_0^2)$ contains: the renormalization factor to a hadronic renormalization scheme and a matching factor between the RGI quark mass M and that renormalized mass $\overline{m}(\mu_{\text{had}})$

$$Z_M^{\text{tm}}(g_0^2) = \frac{M}{\overline{m}(\mu_{\text{had}})} Z_P^{-1}(g_0^2, a\mu_{\text{had}}). \tag{4.33}$$

Notice that, the ratio on the r.h.s. of the equation is independent of the quark flavor as follows from the use of a mass-independent renormalization scheme.

4.3.4 Pseudoscalar Decay Constants

Decay constants contain the non-perturbative contribution to the weak leptonic decay amplitude of flavored mesons. The only matrix element that couples a pseudoscalar state to a weak interaction defines the decay constant f_{qr}

$$\left|\langle 0|\mathcal{A}_0^{qr}|P^{qr}(\boldsymbol{p}=0)\rangle\right| = \frac{f_{qr}M_{qr}}{\sqrt{2M_{qr}L^3}}, \tag{4.34}$$

where the state $|P^{qr}\rangle$ is the ground state for a pseudoscalar meson. The factor $1/\sqrt{2M_{qr}L^3}$ stand for the usual relativistic normalization of one particle states. The symmetries in the Wtm setup allow to compute decay constants just with pseudoscalar-pseudoscalar correlators. Due to the fact that the vector point-split current $\tilde{V}_\mu^{qr}$ (Eq. (3.9)) is exactly normalized and therefore $Z_\mu = Z_P^{-1}$, the renormalized decay constant can be computed without need of any renormalization constant.

The zero-momentum projection reads

$$\langle 0|\partial_0^*\tilde{V}_0^{qr}|P^{qr}(\boldsymbol{p}=0)\rangle = i(\mu_q-\mu_r)\,\langle 0|P^{qr}|P^{qr}(\boldsymbol{p}=0)\rangle\,. \tag{4.35}$$

At full twist, the physical axial current is related to the vector current for non-diagonal flavors that mixes up-type and down-type quarks (see Appendix B)

$$V_\mu^{qr} = -i\mathcal{A}_\mu^{qr}, \quad \mu_q > 0 > \mu_r, \tag{4.36}$$

We apply this relation to the renormalized currents. Hence, the renormalized pseudoscalar decay constant is related to

$$f_{qr}^R = \sqrt{\frac{2L^3}{M_{qr}^3}}\,(|\mu_q|+|\mu_r|)\,|\langle 0|P^{qr}|P^{qr}(\boldsymbol{p}=0)\rangle|\,, \quad \mu_q > 0 > \mu_r. \tag{4.37}$$

We extract the matrix element by fitting pseudoscalar-pseudoscalar correlators $f_{PP}^{q,r}(x_0,y_0)$ to an exponential functional form at large distances, where the exponential decay is dominated by the ground state.

$$f_{PP}^{q,r}(x_0,y_0) \approx a^6L^3\,|\langle 0|P^{qr}|P^{qr}(\boldsymbol{p}=0)\rangle|^2\,e^{-M_{qr}(x_0-y_0)}. \tag{4.38}$$

5 RESULTS

In this chapter we present our results for the charm quark mass and decay constants of pseudoscalar charmed mesons. We describe the chiral and continuum extrapolation strategy for the different observables in Section 5.2. In Section 5.3, we show the numerical results for the physical observables. We follow a similar analysis strategy to the one proposed in [47].

5.1 RUN PARAMETERS AND STRATEGY

We perform simulations on the subset of CLS ensembles listed in Table 3.1. Once the light-strange sector is tuned to maximal twist and matched to the sea (see Section 3.4), we compute light and strange propagators at the target values of (m, μ_l, μ_s). Then, we compute heavy propagators at three different values of the twisted mass mass μ_c^i around the charm region. The computation of charmed observables at different values of the charm quark mass allows to interpolate observables at the physical value of the charm quark mass. In Table 5.1, we specify the run parameters for each ensemble used in the analysis.

Our error analysis is based on the Γ-method [48], a general framework for error analysis of autocorrelated data. We briefly review the Γ-method in Appendix C. The analysis program uses the ADerrors library [3], which implements the Γ-method with Automatic Differentiation (AD) techniques [49]. Automatic Differentiation plays an important role in our analysis, as it provides a simple way to propagate errors of complex functions keeping track of all the covariances. Moreover, AD techniques avoid the numerical computation of derivatives, which may lead to numerical instabilities. We developed a Julia package based on ADerrors for the analysis of QCD observables.

As discussed in Subsection 3.4.1, the matching procedure for the charm quark can be taken into account at the level of analysis. We carry out the charm quark interpolation within the combined chiral and continuum fits. In order to control systematic effects, we perform fits with different models for each observable, and we also impose three different charm matching conditions Eq. (3.30) for each model. We

Id	β	$\kappa_{\rm cr}$	$a\mu_l$	$a\mu_s$	$a\mu_c^1$	$a\mu_c^2$	$a\mu_c^3$
H101	3.40	0.137284	0.006591	0.006591	0.237975	0.250500	0.263025
H102	3.40	0.137299	0.004734	0.010090	0.228285	0.240300	0.252315
H400	3.46	0.137299	0.005913	0.005913	0.204155	0.214900	0.225645
N202	3.55	0.137300	0.005228	0.005228	0.167105	0.175900	0.184695
N203	3.55	0.137312	0.002420	0.01077	0.172805	0.181900	0.190995
N200	3.55	0.137309	0.003640	0.008432	0.173375	0.182500	0.191625
N300	3.70	0.137207	0.004132	0.004132	0.130910	0.137800	0.144690
J303	3.70	0.137213	0.001512	0.009570	0.133000	0.140000	0.147000

Table 5.1: List of run parameters for each ensemble in Table 3.1. $\kappa_{\rm cr}$ is the critical value of the hopping parameter $\kappa_{\rm cr} = 1/(2am_{\rm cr})$. The values on the fourth and fifth columns correspond to matched values of the light and strange twisted mass. The last three columns contain the different values of heavy twisted mass in the charm region.

use a Bayesian model average as proposed in [50] to estimate the systematic errors (see Appendix D). Functional forms for the observables are discussed in next section.

After having extracted the meson masses, the pseudoscalar decay constants and the renormalization group invariant charm quark mass, we express those observables in terms of the reference scale t_0. We multiply all the observables in lattice units by the factor $\sqrt{8t_0/a^2}$ in order to cancel out the explicit dependence on the lattice spacing a. Then, observables in units of t_0 are shifted to the renormalized chiral trajectory $\phi_4 = \phi_4^{\rm phys}$. We determine the values of the mass shift Δm for each ensemble as described in Section 3.3. We apply the mass shift to the charmed observables $\mathcal{O}_c$ as

$$\begin{aligned} \mathcal{O}_c(\phi_4^{\rm phys}) &= \mathcal{O}_c(\phi_4) + \Delta m \sum_f \frac{{\rm d}\mathcal{O}_c}{{\rm d}m_f}, \\ \frac{{\rm d}\mathcal{O}_c}{{\rm d}m_f} &= -\sum_i \frac{\partial \mathcal{O}_c}{\partial \overline{P}_i} \left\langle \left(P_i - \overline{P}_i\right) \left(\frac{\partial S}{\partial m_f} - \frac{\overline{\partial S}}{\partial m_f} \right) \right\rangle . \end{aligned} \tag{5.1}$$

Valence observables only receive one contribution to the mass shift, since they do not depend explicitly on the sea quark masses.

5.2 CHIRAL AND CONTINUUM EXTRAPOLATIONS

After applying the mass shifting, we describe our strategy to extrapolate results to the continuum limit at physical values of the quark masses. We parametrize the RGI charm quark mass in the continuum limit with the following ansatz

$$\sqrt{8t_0}M_c^{\mathrm{RGI}}(0,\phi_2,\phi_c) = p_0 + p_1\phi_2 + p_2\phi_c. \tag{5.2}$$

The extrapolation to the physical point is given by $\phi_2 = 8t_0M_\pi^2$. The renormalized chiral trajectory guarantees that the physical value of the kaon mass is recovered at $\phi_2 = \phi_2^{\mathrm{phys}}$. The physical value of ϕ_2 is computed with the isospin symmetric values of the pion mass in [51] and the physical value of t_0 in [17] (see Section 3.5).

According to heavy quark effective theory [52], the charmed meson masses are expected to behave linearly at leading order with respect to charm quark mass $M_c = m_c[1 + O(1/M_c)]$. We parametrize this dependence with a term linear in ϕ_c. We will use three different values of $\phi_{c,i}$ (Eq. (3.30)) that correspond to different matching conditions for the charm quark. We use the physical values of the charmed meson masses from the PDG [53] to match $\phi_{c,i}$ to their physical value.

To parametrize the dependence on the lattice spacing a, we expect $O(a^2)$ scaling up to small corrections of order $O(a\mathrm{tr}M_{\mathrm{sea}})$. As we have explained in Section 3.2, we expect those corrections to be negligible for lattice spacings $a \lesssim 0.086\,\mathrm{fm}$. We neglect cutoff effects proportional to odd powers of the lattice spacing a.

$$c_M(a,\phi_2,\phi_c) = \frac{a^2}{8t_0}\left(c_1^1 + c_2^1\phi_c^2 + c_3^1\phi_2\right) + \left(\frac{a^2}{8t_0}\right)^2\left(c_1^2 + c_2^2\phi_c^4 + c_3^2\phi_c^2\right). \tag{5.3}$$

We neglect terms proportional $O(a^4M_\pi^4)$ and $O(a^4M_\pi^2)$ in the ansantz because they are expected to be subleading in our power counting.

We use different model parametrizations of c_m. We consider all the combinations[1] terms with coefficients c_i^j, which leads to 2^5 different functional forms for c_M.

For the charm quark mass we consider a linear and non-linear parametrization of the cutoff effects respectively

$$\sqrt{8t_0}M_c^{\mathrm{RGI}}(a,\phi_2,\phi_c) = \sqrt{8t_0}M_c^{\mathrm{RGI}}(0,\phi_2,\phi_c) + c_M(a,\phi_2,\phi_c), \tag{5.4}$$

$$\sqrt{8t_0}M_c^{\mathrm{RGI}}(a,\phi_2,\phi_c) = \sqrt{8t_0}M_c^{\mathrm{RGI}}(0,\phi_2,\phi_c)\left(1 + c_M(a,\phi_2,\phi_c)\right). \tag{5.5}$$

Thus, we end up with 64 ansätze for each matching condition for the charm quark.

[1] In practice, the coefficient c_1^1 is always included.

The decay constants f_D and f_{D_s} are computed in a similar way. By taking advantage of Chiral Perturbation Theory with heavy quarks [54, 55], we can perform global chiral fits for both decay constants. We consider linear chiral fits

$$\sqrt{8t_0} f_D(0,\phi_2,\phi_c) = p_0 + p_1\phi_2 + \frac{p_2}{\sqrt{\phi_c}}, \tag{5.6}$$

$$\sqrt{8t_0} f_{D_s}(0,\phi_2,\phi_c) = p_0 + p_1(2\phi_4 - 2\phi_2) + \frac{p_2}{\sqrt{\phi_c}}, \tag{5.7}$$

and fits including chiral logarithm corrections

$$\sqrt{8t_0} f_D(0,\phi_2,\phi_c) = \tilde{p}_0 + \tilde{p}_1\phi_2 + \frac{\tilde{p}_2}{\sqrt{\phi_c}} + \tilde{p}_3\left(3\mu_\pi + 2\mu_K + \frac{1}{3}\mu_\eta\right), \tag{5.8}$$

$$\sqrt{8t_0} f_{D_s}(0,\phi_2,\phi_c) = \tilde{p}_0 + \tilde{p}_1(2\phi_4 - 2\phi_2) + \frac{\tilde{p}_2}{\sqrt{\phi_c}} + \tilde{p}_3\left(4\mu_K + \frac{4}{3}\mu_\eta\right), \tag{5.9}$$

where μ_π, μ_K and μ_η are written in terms of ϕ_2 and ϕ_4 as follows

$$\mu_\pi(\phi_2) = \phi_2 \ln(\phi_2), \tag{5.10}$$

$$\mu_K(\phi_2) = \left(\phi_4 - \frac{1}{2}\phi_2\right)\ln\left(\phi_4 - \frac{1}{2}\phi_2\right), \tag{5.11}$$

$$\mu_\eta(\phi_2) = \left(\frac{4}{3}\phi_4 - \phi_2\right)\ln\left(\frac{4}{3}\phi_4 - \phi_2\right). \tag{5.12}$$

We consider a similar parametrization for the cutoff effects to c_M. However, fits that include the non-linear term in the combined fit turn out to be more unstable. We thus only consider the linear combination of cutoff effects for the decay constants, and end up with 64 different ansäntze for the combined fit for each matching condition.

$$\sqrt{8t_0} f_{D_{(s)}}(a,\phi_2,\phi_c) = \sqrt{8t_0} f_{D_{(s)}}(0,\phi_2,\phi_c) + c_{f_{(s)}}(a,\phi_2,\phi_c), \tag{5.13}$$

$$c_f(a^2,\phi_2,\phi_c) = \frac{a^2}{8t_0}\left(c_1^1 + c_2^1\phi_c^2 + c_3^1\phi_2\right) + \left(\frac{a^2}{8t_0}\right)^2\left(c_1^2 + c_2^2\phi_c^4 + c_3^2\phi_c^2\right), \tag{5.14}$$

$$c_{f_s}(a^2,\phi_2,\phi_c) = \frac{a^2}{8t_0}\left(c_1'^1 + c_2'^1\phi_c^2 + c_3'^1\phi_2\right) + \left(\frac{a^2}{8t_0}\right)^2\left(c_1'^2 + c_2'^2\phi_c^4 + c_3'^2\phi_c^2\right). \tag{5.15}$$

We apply linear chiral fits to extract the η_c decay constant (neglecting disconnected contributions) following a similar strategy.

Additionally, we study the ratio of f_{D_s} and f_D. We expand the ratio of decay constants at first order

$$\frac{f_{D_s}}{f_D}(a,\phi_2) = 1 + p_1\left(\phi_4 - \frac{3}{2}\phi_2\right) + c_1\frac{a^2}{8t_0} + c_2\frac{a^2}{8t_0}\phi_2, \tag{5.16}$$

which does not depend on ϕ_c. We only take into account cutoff effects of order $O(a^2)$ and $O(a^2 M_\pi^2)$. Cutoff effects proportional to ϕ_c are suppressed in the ratio. Notice that the ratio is 1 by construction in the symmetric point ($M_\pi = M_K$). Therefore, symmetric point ensembles do not contribute to the fit but the latter is strongly constrained by the nature of our chiral trajectory.

Fit parameter estimation can be problematic for highly correlated data [56, 57]. The estimation of the covariance matrix requires large samples and the matrix inverse is completely dominated by the small modes. Fit parameters can be computed minimizing uncorrelated χ^2, which provides a reliable estimation for the fit parameters with highly correlated data. Nevertheless, the χ^2 value is no longer a measure of the quality of the fit. In order to quantify the goodness-of-fit, we thus use the χ^2 expected χ^2_{exp} [58], the expected χ^2 value for the estimated model parameters. The ratio $\chi^2/\chi^2_{\text{exp}}$ is a good measure of the fit quality, and therefore we introduce a corrected χ^2 [47]

$$\chi^2_{\text{corr}} = (\text{d.o.f.})\frac{\chi^2}{\chi^2_{\text{exp}}}, \tag{5.17}$$

where $\chi^2_{\text{corr}}/(\text{d.o.f.}) \approx 1$ is a good measure for the likelihood of the data describing the model. Fit parameters are extracted through minimization of an uncorrelated χ^2. The value of χ^2_{corr} provides a weight to each model in the model average as described in Appendix D.

5.3 PHYSICAL RESULTS

Following the procedure described in the previous sections, we compute the RGI charm quark mass and the decay constants f_D and f_{D_s}. We present continuum and chiral extrapolations for those observables for the preferred model and matching condition as given by the Akaike Information Criteria (AIC) (see Appendix D). Similar plots for different matching conditions can be found in Appendix E.

The behavior of matching conditions along the chiral trajectory is non-trivial. The values of ϕ_c depend on the values of the light-strange quark masses and therefore physical observables from different matching conditions are only expected to agree in the continuum and at ϕ_2^{phys}. In order to validate our matching strategy, we check the results for each matching condition for the charm quark mass, which is specially sensitive to the matching procedure. Results can be found in Table 5.2, where the errors are statistical and systematic, respectively. Values correspond to model averages of 64 models as described in the previous section. In figure 5.1, we show the continuum extrapolation for the three different matching conditions with the

preferred models. We check that results from flavor average and η_c are compatible at the 1-σ level.

Matching	$\phi_{c,1}^{\text{phys}}$	$\phi_{c,2}^{\text{phys}}$	$\phi_{c,3}^{\text{phys}}$	combined
$\sqrt{8t_0}M_c^{\text{RGI}}$	3.141(53)(6)	3.276(59)(52)	3.150(49)(13)	3.169(52)(50)

Table 5.2: Results of the Bayesian model average of the RGI charm quark mass for the three different matching conditions $\phi_{c,i}$. The last column corresponds to the combined result.

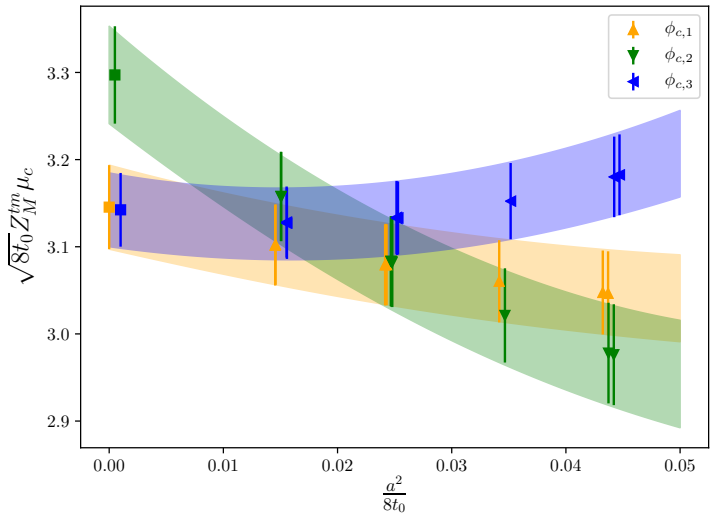

Figure 5.1: Continuum extrapolation of the RGI charm quark mass. Points represent values of the charm quark mass interpolated with different matching conditions. The fits correspond the preferred model for each matching condition.

We observe that fits with the matching condition $\phi_{c,2}$ have higher systematic effects that are related to the determination of the vector states. This effect may be related to contamination with excited states. Since there is tension with respect the other conditions and fits present higher $\chi^2_{\text{corr}}/(\text{d.o.f.})$, we decide to discard results related to the spin-flavor average for that reason.

In Figure 5.2, we show the chiral and continuum extrapolations for the RGI mass for the preferred model and the flavor average. We observe a smooth $O(a^2)$ scaling in the charm quark mass. We also recognize a smooth linear dependence on ϕ_2 as expected. The values of $\chi^2_{\text{corr}}/(\text{d.o.f.}) \approx 0.3$

Systematic effects related to the Bayesian model average are plotted in Figure 5.3. One can recognize that the distribution function is unimodal and its maximum corresponds to the best model with the highest weight.

After combining the results from $128(64 \times 2)$ models, we quote:

$$M_c^{\mathrm{RGI}}(N_f = 3) = 1.500(16)(5)\,\mathrm{GeV}. \tag{5.18}$$

The first error is statistical while the second error is related to systematics.

We make use of perturbation theory to give the result in the $\overline{\mathrm{MS}}$ scheme for $N_f = 4$. The perturbative calculations are performed with the program RunDec [59–61] at five-loops. Renormalization group equations are solved with the value of $\Lambda^{(3)}_{\overline{\mathrm{MS}}} = 338(12)\,\mathrm{MeV}$ from [62], which allows to extract the mass in the $\overline{\mathrm{MS}}$ scheme from the RGI mass in the three-flavor theory. Then, we match the $N_f = 3$ and $N_f = 4$ theories at the energy scale of the scale invariant charm quark mass $\overline{m}_c(\mu = \overline{m}_c, N_f = 3)$. So, we can compute the $\overline{\mathrm{MS}}$ charm quark mass in the four-flavor theory. We provide the RGI mass and the quark mass in the $\overline{\mathrm{MS}}$ scheme for $N_f = 4$. We quote the results:

$$\begin{aligned} \overline{m}_c(\mu = 3\,\mathrm{GeV}, N_f = 4) &= 1.013(11)(8)_\Lambda\,\mathrm{GeV}, & (5.19)\\ \overline{m}_c(\mu = \overline{m}_c, N_f = 4) &= 1.297(10)(13)_\Lambda\,\mathrm{GeV}, & (5.20)\\ M_c^{\mathrm{RGI}}(N_f = 4) &= 1.565(18)(2)_\Lambda\,\mathrm{GeV}, & (5.21) \end{aligned}$$

where the first error comes from the error in $M_c^{\mathrm{RGI}}(N_f = 3)$ and the second error arises from the uncertainty in $\Lambda^{(3)}_{\overline{\mathrm{MS}}}$.

For the decay constants we show in Figures 5.4 and 5.6 the continuum and chiral extrapolations for the model with higher likelihood. The preferred model shows linear chiral dependence and cutoff effects of order $O(a^2)$. We do not resolve chiral logarithms for the set of ensembles used in the analysis. Figure 5.8 shows the chiral extrapolations including logarithmic contributions. We also discern from the figures on the left a small dependence on ϕ_c in our range of charm mass parameters. The fit with higher weight in the model average has a value of $\chi^2_{\mathrm{corr}}/(\mathrm{d.o.f.}) \approx 0.8$. In Figure 5.5 and 5.7 we exhibit the Bayesian model averages and the histograms.

For the combined fits of both decay constants, we quote

$$\begin{aligned} f_D &= 212.3(6.0)(3.1)\,\mathrm{MeV}, & (5.22)\\ f_{D_s} &= 243.5(4.2)(1.6)\,\mathrm{MeV}. & (5.23) \end{aligned}$$

The error budget for the charm quark mass and decay constants f_D and f_{D_s} is given in Figure 5.9. The error of the decay constants is completely dominated by statistical uncertainty of correlators and the resulting errors on chiral and continuum

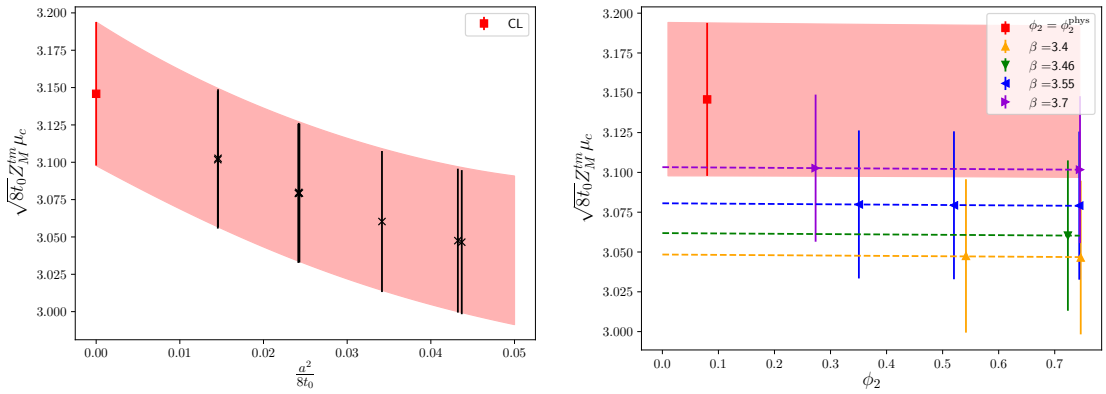

Figure 5.2: *Left*: Continuum limit extrapolation of the RGI charm quark mass $M_c^{\mathrm{RGI}}(N_f = 3)$ in terms of the reference scale t_0. The red band represent the projection to the physical point $\phi_2 = \phi_2^{\mathrm{phys}}$ and $\phi_c = \phi_c^{\mathrm{phys}}$. *Right*: Chiral extrapolation of the RGI charm quark mass $M_c^{\mathrm{RGI}}(N_f = 3)$ in terms of the reference scale t_0. The red band represents the projection to the continuum limit. Dashed lines correspond to chiral extrapolations at finite lattice spacing. The results of both plots are matched to $\phi_{c,1}^{\mathrm{phys}}$.

fits. As described in Section 4.3, we compute decay constants without requiring renormalization constants. Renormalization constants introduce the main source of uncertainty in the RGI quark mass in addition to the scale setting procedure and two-point correlation functions. Notice that the uncertainty of the charm quark mass in the $\overline{\mathrm{MS}}$ scheme at the charm scale is dominated by contributions coming from perturbation theory, reflecting the use of perturbation theory at few-GeV scale. The addition of more ensembles with finer lattice spacing and lower pion masses could reduce the uncertainty coming from chiral and continuum extrapolations for all the observables in the study.

We also consider the ratio of decay constants.

$$\frac{f_{D_s}}{f_D} = 1.1655(60). \tag{5.24}$$

We do not quote a systematic error estimation for the ratio because we do not have enough ensembles outside the symmetric point to perform a Bayesian model average. In Figure 5.12, we show the chiral fit with a value $\chi^2/\chi^2_{\mathrm{exp}} \approx 0.7$. The ratio is less sensitive to lattice artifacts since the bulk of discretization effects are canceled. We observe linear dependence on ϕ_2 for the ratio.

In Figures 5.10 and 5.11, we present a comparison between our results and the Flavor Lattice Averaging Group (FLAG) summary plots [62]. The value of the charm quark mass in the $\overline{\mathrm{MS}}$ scheme at $\mu = \overline{m}_c$ present a 1-sigma tension with respect

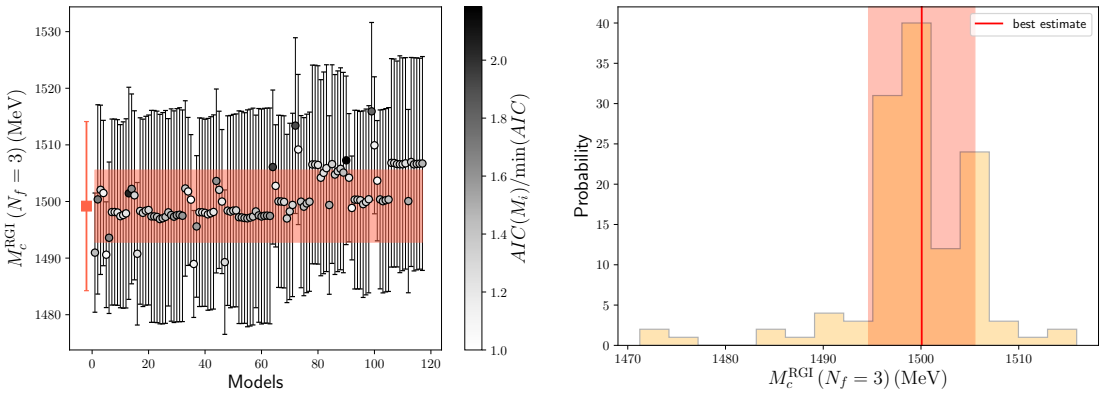

Figure 5.3: *Left*: Model average of $M_c^{\mathrm{RGI}}(N_f = 3)$. The red band represent the systematic error and the red point represents the model average with the total error. *Right*: Histogram with the results of each model of $M_c^{\mathrm{RGI}}(N_f = 3)$. The red band represents the systematic error.

to the FLAG average at $N_f = 2 + 1$, dominated by HPQCD 10 [63]. Our result is compatible within 1-σ errors with ALPHA 21 [47], which carries out a similar analysis strategy. The result is also compatible with other lattice computations such as JLQCD 16 [64] and χQCD 14 [65].

The value f_D is in agreement with the FLAG average and the uncertainties are similar to RBC/UKQCD 17 [66] and HPQCD 12 [67]. We observe a 1-σ dispersion for our determination of f_{D_s} with respect to the FLAG average. The independent determination of the ratio f_{D_s}/f_D is also 1-sigma below the average and it is consistent with the independent computations of f_D and f_{D_s}.

We also compute the results for the decay constant of the connected contribution of the η_c meson. A very smooth dependence on ϕ_2 in the chiral extrapolation is seen, as expected. In figure 5.13, we show the continuum and chiral extrapolations for the connected contribution to the η_c decay constant with a value of $\chi^2_{\mathrm{corr}}/(\mathrm{d.o.f.}) \approx 1.0$. We observe large scaling violations well described by a linear behavior in a^2, and a smooth dependence on the pion mass as expected since the η_c meson does not depend on valence light-strange quarks. We quote the value for the $64(32 \times 2)$ models:

$$f_{\eta_c} = 382.7(3.5)(2.5)\,\mathrm{MeV}. \tag{5.25}$$

Our results is more than 2 sigma away from other lattice computation at $N_f = 2 + 1$ (HPQCD [88]). Further preliminary results for the charmonium sector can be found in [98].

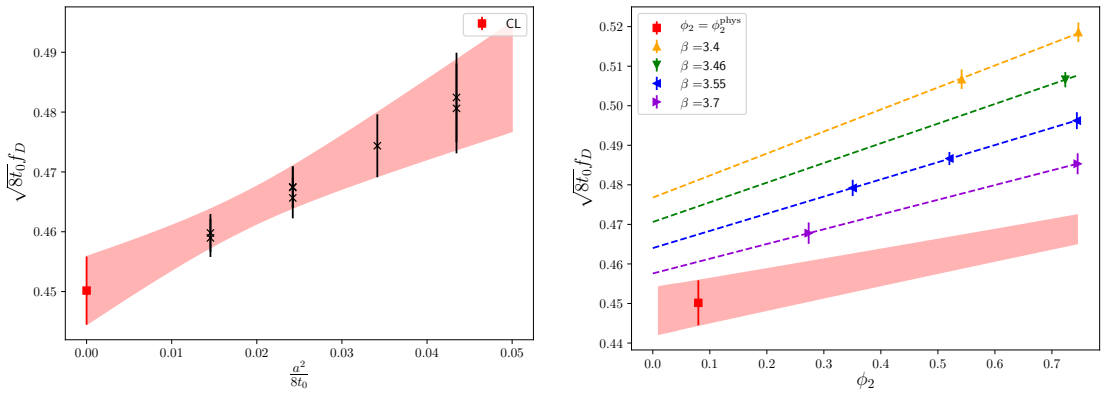

Figure 5.4: *Left*: Continuum limit extrapolation of the decay constant f_D in units of the reference scale t_0. The red band represent the projection to the physical point $\phi_2 = \phi_2^{\rm phys}$ and $\phi_c = \phi_c^{\rm phys}$. *Right*: Chiral extrapolation of the decay constant f_D in units of the reference scale t_0. The red band represents the projection to the continuum limit. Dashed lines correspond to chiral extrapolations at finite lattice spacing. The results of both plots are matched to $\phi_{c,1}^{\rm phys}$.

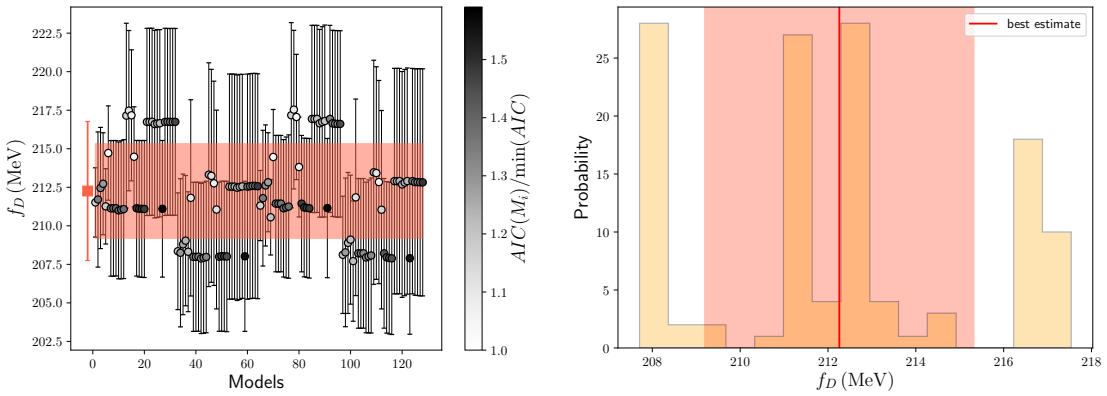

Figure 5.5: *Left*: Model average of f_D. The red band represent the systematic error and the red point represents the model average with the total error. *Right*: Histogram with the results of each model and each matching condition of f_D. The red band represents the systematic error.

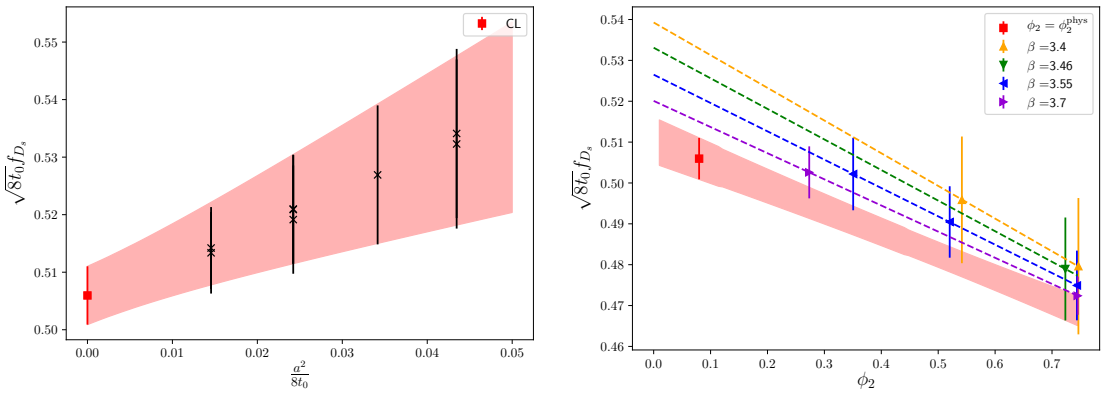

Figure 5.6: *Left*: Continuum limit extrapolation of the decay constant f_{D_s} in units of the reference scale t_0. The red band represent the projection to the physical point $\phi_2 = \phi_2^{\text{phys}}$ and $\phi_c = \phi_c^{\text{phys}}$. *Right*: Chiral extrapolation of the decay constant f_{D_s} in units of the reference scale t_0. The red band represents the projection to the continuum limit. Dashed lines correspond to chiral extrapolations at finite lattice spacing. The results of both plots are matched to $\phi_{c,1}^{\text{phys}}$.

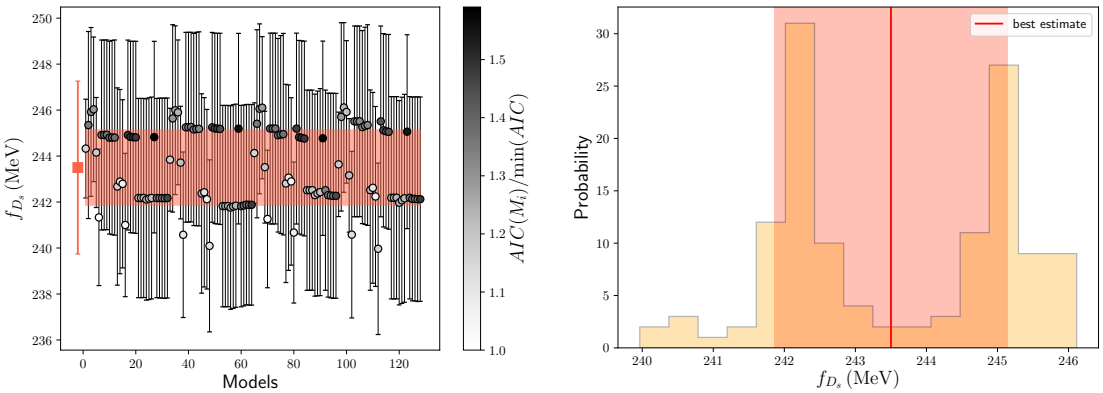

Figure 5.7: *Left*: Model average of f_{D_s}. The red band represent the systematic error and the red point represents the model average with the total error. *Right*: Histogram with the results of each model and each matching condition of f_{D_s}. The red band represents the systematic error.

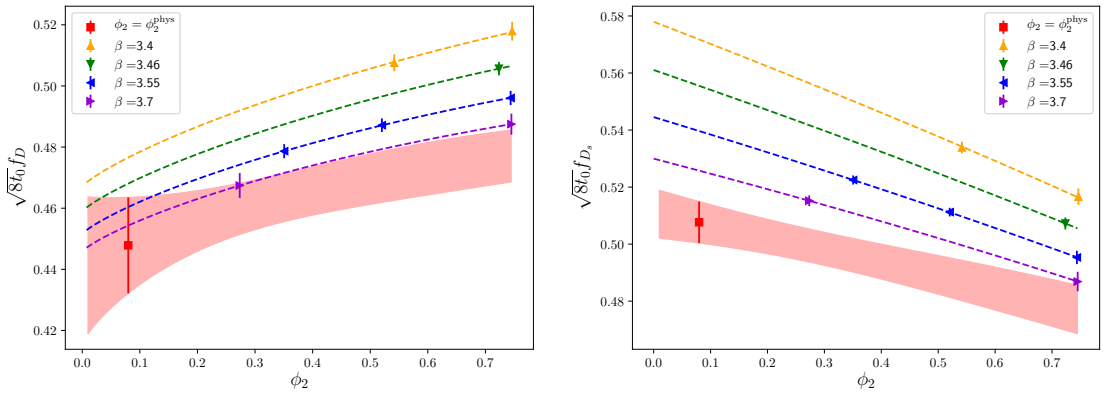

Figure 5.8: Chiral extrapolations of the decay constants f_D and f_{D_s} in terms of the scale t_0. The red band represents the projection to the continuum limit. Dashed lines correspond to chiral extrapolations at finite lattice spacing. The functional form contains chiral logarithms. The results of both plots are matched to $\phi_{c,1}^{\rm phys}$.

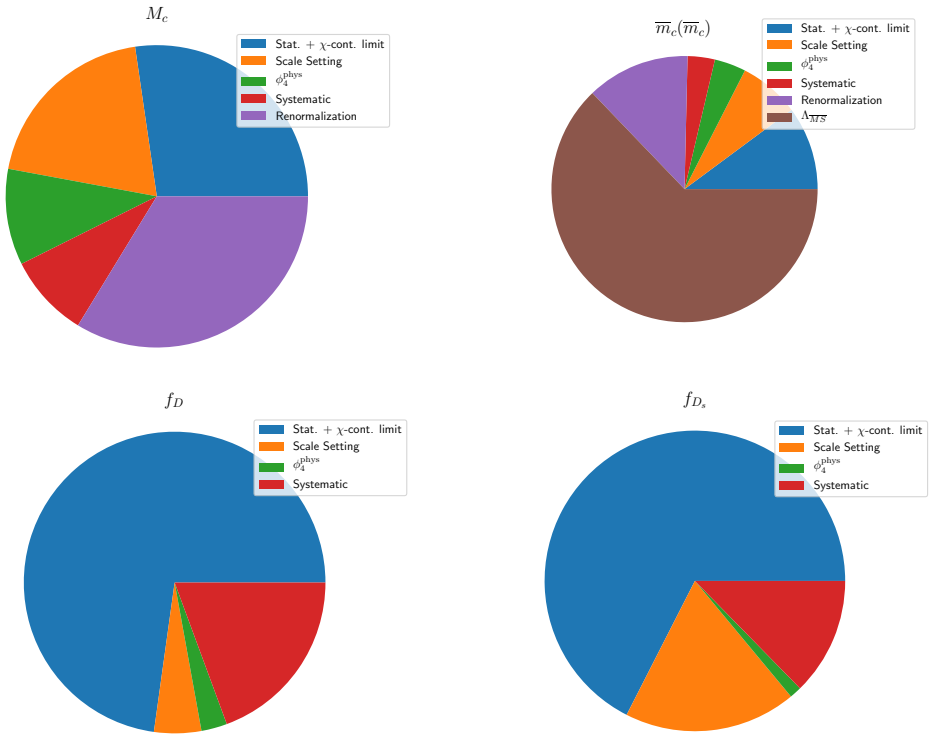

Figure 5.9: Error contributions for the final results of $M_c^{\rm RGI}$, f_D and f_{D_s}.

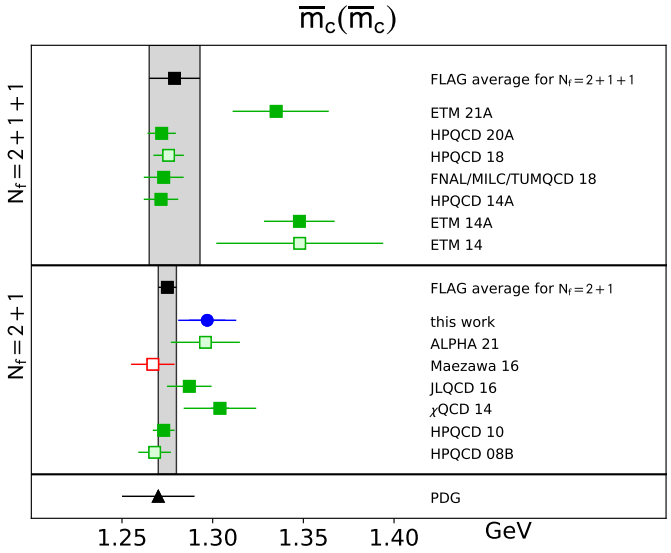

Figure 5.10: Comparison of the charm quark mass and decay constants with respect to the FLAG average [47, 53, 62–65, 68–77]. The blue points correspond to our study. Charm quark mass $\overline{m}_c$ in the $\overline{\text{MS}}$ scheme at the scale $\mu = \overline{m}_c$ in GeV.

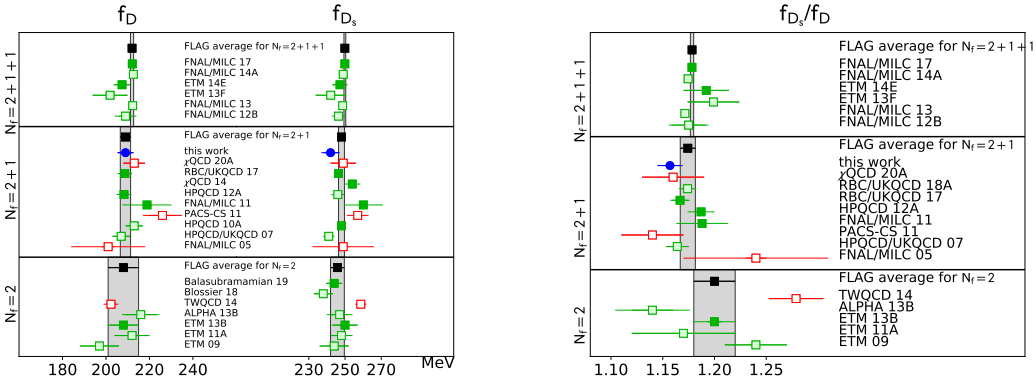

Figure 5.11: Comparison of the decay constants and the ratio f_{D_s}/f_D with respect to the FLAG average [62, 65–67, 78–97]. The blue points correspond to our study. *Left:* Decay constants f_D and f_{D_s} in MeV. *Right:* Ratio f_{D_s}/f_D.

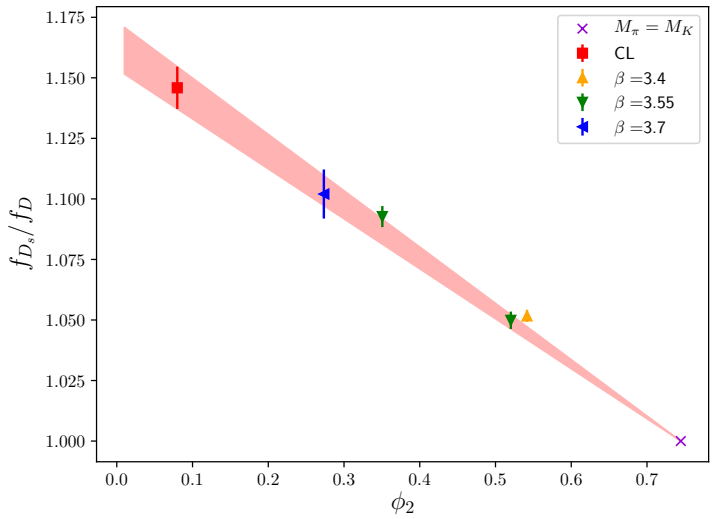

Figure 5.12: Chiral extrapolation of the ratio f_{D_s}/f_D. The red band represent the projection to the continuum limit.

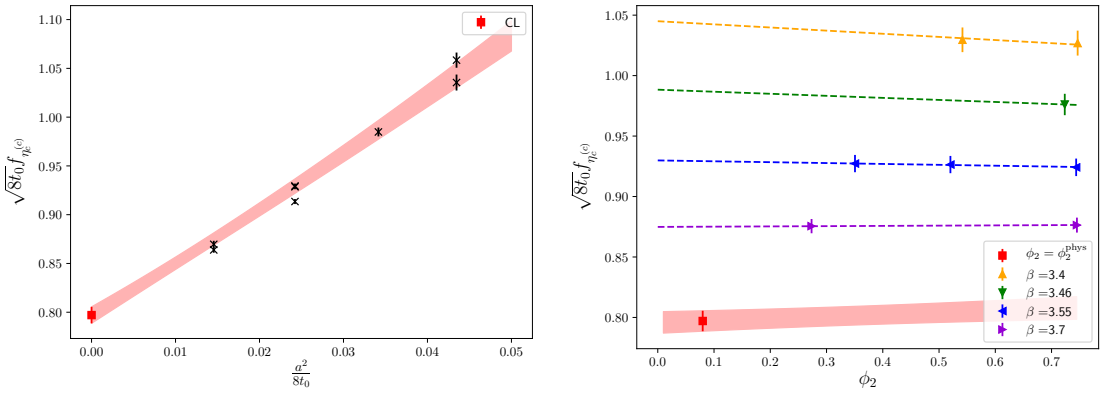

Figure 5.13: *Left*: Continuum limit extrapolation of the decay constant f_{η_c} in units of the reference scale t_0. The red band represent the projection to the physical point $\phi_2 = \phi_2^{\rm phys}$ and $\phi_c = \phi_c^{\rm phys}$. *Right*: Chiral extrapolation of the decay constant f_{η_c} in units of the reference scale t_0. The red band represents the projection to the continuum limit. Dashed lines correspond to chiral extrapolations at finite lattice spacing. The results of both plots are matched to $\phi_{c,1}^{\rm phys}$.

6 CONCLUSIONS

In this work we have studied a lattice field theory regularization on QCD with a mixed action. We describe the setup of Wilson $O(a)$-improved fermions in the sea and Wilson twisted mass fermions at full twist in the valence sector. The valence action guarantees automatic $O(a)$-improvement for the desired quantities up to residual $O(aM_{\text{sea}})$ cutoff effects that are expected to be negligible at the current level of precision. Mixed-action setups require a matching procedure between sea and valence in order to recover unitarity in the continuum limit. We detail a tuning procedure to match light-strange quarks while the twist angle is fixed to $\pi/2$. In contrast to the light sector, the charm quark is quenched and therefore it only needs to be matched to a physical observable. The charm matching condition at finite lattice spacing introduce a dependence on a physical scale, *e.g.*, t_0^{phys}. We treat the matching of the charm quark in combination with the chiral and continuum extrapolations in global fits to our data.

We present an analysis with a subset of CLS ensembles with four values of the lattice spacing within the range $0.05\,\text{fm} \lesssim a \lesssim 0.087\,\text{fm}$ (*i.e.*, $0.0025\,\text{fm}^2 \lesssim a^2 \lesssim 0.0076\,\text{fm}^2$) and pion masses between 260 MeV and 420 MeV. We compute for each ensemble three heavy propagators with masses around the charm quark mass. Therefore, charm observables can be matched to their physical value by performing interpolations. We use Distance Preconditioning techniques on heavy propagators in order to deal with precision loss at large distances.

We determine the values of the charm quark mass and decay constants of D and D_s mesons. We take advantage of Heavy Quark Effective Theory (HQET) and Chiral Perturbation Theory (χPT) with heavy mesons to parametrize the chiral-continuum extrapolation combined with the charm scale interpolation. Systematic effects are estimated in the context of Bayesian statistics. We use a Bayesian model average with different functional forms to provide a measure of the systematic effects. Additionally, we introduce in the analysis three different matching condition for the charm mass. The charm quark mass is tuned by imposing the physical values of meson mass combinations. For that purpose, we consider the flavor average, spin-flavor average and the η_c meson mass (neglecting disconnected contributions).

We observe that models that contain dependence on the spin-flavor average turn out to have larger values of χ^2. We use a model average based on the Akaike Information Criteria (AIC) using 64 functional forms and the two other matching conditions for each observable. We quote our final result for the Renormalization Group Invariant (RGI) quark mass in the three-flavor theory

$$M_c^{\rm RGI}(N_f = 3) = 1.500(16)(5)\,{\rm GeV},$$

and we use perturbation theory at 5-loops to compute the charm quark mass in the $\overline{\rm MS}$ scheme in the four-flavor theory

$$\overline{m}_c(\overline{m}_c) = 1.297(10)(13)_\Lambda\,{\rm GeV},$$

which is well compatible with other lattice $N_f = 2 + 1$ determinations [47, 64, 65].

Decay constants f_D and f_{D_s} are determined using global fits and ansätze based on χPT with heavy mesons. We take into account different model with and without chiral logarithmic corrections. We quote the following results for the decay constants

$$f_D = 212.3(6.0)(3.1)\,{\rm MeV}, \qquad f_{D_s} = 243.5(4.2)(1.6)\,{\rm MeV}.$$

CONCLUSIONES

En este trabajo estudiamos una regularización de QCD de teoría de campos en el retículo con una acción mixta. Describimos el montaje de fermiones de Wilson mejorados a $O(a)$ en el mar y fermiones Wilson twisted mass a twist máximo en el sector de valencia. La acción de valencia garantiza el mejorado automático a $O(a)$ para las cantidades deseadas salvo por efectos residuales de cutoff $O(aM_{\text{sea}})$, que se espera que sean despreciables con el nivel de precisión actual. Los montajes con acciones mixtas requieren de un proceso de matching entre mar y valencia para recuperar la unitariedad en el límite continuo. Detallamos un proceso de calibrado para imponer igualdad de masas en los quarks ligeros y strange mientras que el ángulo de twist se fija a $\pi/2$. A diferencia del sector ligero, la masa del quark charm no se encuentra en el mar, y por lo tanto solo necesita coincidir con un observable físico. La condición de matching del quark charm a espaciado reticular finito introduce una dependencia en una escala física *e.g.*, t_0^{phys}. Tratamos el matching del quark charm en combinación con las extrapolaciones quirales al continuo.

Presentamos un análisis con un subconjunto de ensembles CLS con cuatro valores de el espaciado reticular en el rango $0.05\,\text{fm} \lesssim a \lesssim 0.087\,\text{fm}$ (*i.e.*, $0.0025\,\text{fm}^2 \lesssim a^2 \lesssim 0.0076\,\text{fm}^2$) y masas de pion entre 260 MeV y 420 MeV. Calculamos en cada ensemble tres propagadores pesados con masas cercanas a la masa del quark charm. Por lo tanto, los observables que depende de este quark pueden ser fijados a su valor físico haciendo interpolaciones. Usamos técnicas de Distance Preconditioning en los propagadores pesados para prevenir la perdida de precisión a distancias grandes.

Determinamos los valores de la masa del quark charm y de las constantes de desintegración de los mesones D y D_s. Aprovechamos la Teoría Efectiva de Quarks Pesados (HQET) y Teoría de Perturbaciones Quirales (χPT) con mesones pesados para parametrizar las extrapolaciones quirales al continuo en combinación con la interpolación a la escala del quark charm. Los efectos sistemáticos son estimados en el contexto de la estadística Bayesiana. Usamos una media de modelos Bayesiana con diferentes formas funcionales para dar una medida de los efectos sistemáticos. Adicionalmente, introducimos en el análisis tres condiciones de matching distintas para el quark charm. La masa de este quark se calibra mediante la imposición de los valores físicos de las combinaciones de masa. Para este propósito consideramos la media de sabor, la media de spin-sabor y la masa del meson η_c (despreciando contribuciones disconexas).

Observamos que los modelos que contienen dependencia en la media de spin-sabor resultan tener valores mayores de χ^2. Usamos una media de modelos basada en el Criterio de Información de Akaike (AIC) usando 64 formas funcionales y las otras dos condiciones de matching para cada observable. Damos un resultado para la masa de quark Invariante del Grupo de Renormalización (RGI) en la teoría de tres sabores

$$M_c^{\mathrm{RGI}}(N_f = 3) = 1.500(16)(5)\,\mathrm{GeV},$$

y usamos teoría de perturbaciones a 5 bucles para calcular la masa del quark charm en el esquema $\overline{\mathrm{MS}}$ en la teoría de cuatro sabores

$$\overline{m}_c(\overline{m}_c) = 1.297(10)(13)_\Lambda\,\mathrm{GeV},$$

la cuál es compatible con otras determinaciones $N_f = 2 + 1$ en el retículo [47, 64, 65].

Las constantes de desintegración f_D y f_{D_s} se determinan usando ajustes globales y formas funcionales basadas en χPT con mesones pesados. Tomamos en consideración diferentes modelos con y sin logaritmos quirales. Damos el siguiente resultado para las constantes de desintegración

$$f_D = 212.3(6.0)(3.1)\,\mathrm{MeV}, \qquad f_{D_s} = 243.5(4.2)(1.6)\,\mathrm{MeV}.$$

ACKNOWLEDGMENTS

En primer lugar quiero dar las gracias a Carlos por todo el tiempo empleado en mi formación y por ser la persona que me acogió en el mundo de la Física cuando era un estudiante de máster. Gracias por todo tipo de charlas variopintas entre reunión y reunión. También quiero agradecerle a Gregorio haber codirgido en la práctica mi doctorado.

I would like to thank to the members of the IFT lattice group, for all the valuable discussions. I would like to specially thank José, Andrea and Alessandro for all the debugging and testing afternoons at the IFT.

Gracias a Víctor por haberme introducido en la Física Teórica y mostrarme con entusiasmo lo que era un doctorado. Gracias por todo lo que me has enseñado. También tengo que agradecer a Miguel, Xabi e Irene, que junto con Víctor me inspiraron para hacer un doctorado.

Hablando de gente del IFT, tengo que dar las gracias a muchas personas por tantos momentos geniales dentro y fuera de la universidad. Gracias Claudia, Javi, Gallego, Salva, Judit, Fernando, Álvaro, Raquel y Guille por todas las comidas y cenas que hemos compartido, y por todos los viajes y excursiones que hemos hecho. Gracias al equipo de pingpong del IFT por todas las reuniones después de comer. Gracias a Claudia, Javi y Guille por haberme dado unos años geniales compartiendo piso. Gracias especialmente a Claudia por acompañarme desde el primer minuto de la carrera hasta este momento, sin tu ayuda no hubiese llegado hasta aquí.

Tengo que mencionar a Guille y Jacobo, mis profes del deporte vertical por haberme enseñado a empujar mis límites tanto físicos como psicológicos. Vuestras enseñanzas siempre son valiosas después de un día largo de trabajo.

Gracias a Pablo y a Iván por haber estado ahí siempre después de tantos años y por las incontables experiencias que hemos vivido (y que sin duda viviremos). Gracias por haberme acompañado prácticamente toda la vida. También tengo que agradecer a toda La Yedra por todos años que hemos pasado juntos, y con los que he crecido.

Tengo que dar las gracias a mis tíos por haberme cuidado durante tantos años y haberme enseñado tantas cosas. Gracias por darme el sentimiento aventurero y haberme enseñado a disfrutar de la naturaleza.

Gracias a mi familia cartagenera por haberme acogido como uno más de la familia y por haberme ayudado en la última etapa de este proyecto.

A mis padres les tengo que agradecer todo. Gracias por todo el apoyo que me habéis dado desde siempre. Soy la persona en la que me he convertido gracias a vosotros. Gracias a mi madre por enseñarme el significado de optimismo y perseverancia. Y gracias a mi padre por haber cuidado de mí en los momentos más tristes.

Y por último y más importante, quiero dar las gracias a Elena. La persona que ha estado presente en los momentos más duros de mi vida. Gracias por apoyarme en cada momento y evitar que tire la toalla, sin tu ayuda este proyecto jamás hubiese salido adelante. Gracias por hacer que crezca como persona con cada día que paso a tu lado.

A CONVENTIONS

GAMMA MATRICES

Dirac matrices in the Euclidean space satisfy

$$\{\gamma_\mu, \gamma_\nu\} = 2\delta_{\mu\nu}\mathbb{1}, \quad \gamma_\mu = \gamma_\mu^\dagger. \tag{A.1}$$

The γ_5 matrix is defined as

$$\gamma_5 = \gamma_0\gamma_1\gamma_2\gamma_3, \tag{A.2}$$

fulfilling the properties

$$\{\gamma_5, \gamma_\mu\} = 0, \quad \gamma_5^2 = \mathbb{1}, \quad \gamma_5 = \gamma_5^\dagger, \tag{A.3}$$

In the Weyl representation, gamma matrices take the form

$$\gamma_0 = \begin{pmatrix} 0 & -\mathbb{1} \\ -\mathbb{1} & 0 \end{pmatrix}, \quad \gamma_k = \begin{pmatrix} 0 & -i\sigma_k \\ i\sigma_k & 0 \end{pmatrix}, \quad \gamma_5 = \begin{pmatrix} \mathbb{1} & 0 \\ 0 & -\mathbb{1} \end{pmatrix}, \tag{A.4}$$

where σ_k $(k = 1, 2, 3)$ are the Pauli matrices. The hermitian tensor $\sigma_{\mu\nu} \equiv \frac{i}{2}[\gamma_\mu, \gamma_\nu]$ in the Weyl representation reads

$$\sigma_{0k} = \begin{pmatrix} \sigma_k & 0 \\ 0 & -\sigma_k \end{pmatrix}, \quad \sigma_{ij} = -\varepsilon_{ijk}\begin{pmatrix} \sigma_k & 0 \\ 0 & \sigma_k \end{pmatrix}. \tag{A.5}$$

DIRAC BILINEARS

We introduce the notation for the Dirac bilinears in the twisted mass basis $\{\chi, \bar{\chi}\}$

$$\begin{aligned} S^{qr}(x) &= \bar{\chi}^q(x)\chi^r(x), & P^{qr}(x) &= \bar{\chi}^q(x)\gamma_5\chi^r(x), \\ V_\mu^{qr}(x) &= \bar{\chi}^q(x)\gamma_\mu\chi^r(x), & A_\mu^{qr}(x) &= \bar{\chi}^q(x)\gamma_\mu\gamma_5\chi^r(x), \\ T_{\mu\nu}^{qr}(x) &= \bar{\chi}^q(x)\sigma_{\mu\nu}\chi^r(x). \end{aligned} \tag{A.6}$$

In a similar way, Dirac bilinears in the physical basis $\{\psi, \bar{\psi}\}$ take the form

$$\begin{aligned} \mathcal{S}^{qr}(x) &= \bar{\psi}^q(x)\psi^r(x), & \mathcal{P}^{qr}(x) &= \bar{\psi}^q(x)\gamma_5\psi^r(x), \\ \mathcal{V}^{qr}_\mu(x) &= \bar{\psi}^q(x)\gamma_\mu\psi^r(x), & \mathcal{A}^{qr}_\mu(x) &= \bar{\psi}^q(x)\gamma_\mu\gamma_5\psi^r(x), \\ \mathcal{T}^{qr}_{\mu\nu}(x) &= \bar{\psi}^q(x)\sigma_{\mu\nu}\psi^r(x). \end{aligned} \tag{A.7}$$

We recall the change of basis in our setup

$$\psi = e^{-i\frac{\pi}{2}\frac{T}{2}\gamma_5}\chi, \quad \bar{\psi} = \bar{\chi}e^{-i\frac{\pi}{2}\frac{T}{2}\gamma_5}, \quad T = \mathrm{diag}(+1,-1,-1,+1). \tag{A.8}$$

B CHIRAL ROTATIONS

We summarize the change of basis between the twisted $\{\chi, \bar{\chi}\}$ and physical basis $\{\psi, \bar{\psi}\}$ for the whole set of Dirac bilinears in our setup. We recall the twisted mass matrix from Section 3.2

$$\boldsymbol{\mu} = \mathrm{diag}(\mu_u, \mu_d, \mu_s, \mu_c) = \mathrm{diag}\,(+|\mu_l|, -|\mu_l|, -|\mu_s|, +|\mu_c|) \tag{B.1}$$

and the relation between both basis in our setup

$$\psi = e^{-i\frac{\pi}{2}\frac{T}{2}\gamma_5}\chi, \quad \bar{\psi} = \bar{\chi}e^{-i\frac{\pi}{2}\frac{T}{2}\gamma_5}, \quad T = \mathrm{diag}(+1, -1, -1, +1). \tag{B.2}$$

We define the sign of the twisted mass for a given flavor such that

$$\eta_q = \mathrm{sgn}(\mu_q). \tag{B.3}$$

Therefore, Dirac bilinears transform into the physical basis $\{\chi, \bar{\chi}\} \to \{\psi, \bar{\psi}\}$ as follows:

$$S^{qr}(x) = \frac{1}{2}(1 - \eta_q\eta_r)\mathcal{S}^{qr}(x) + \frac{i}{2}(\eta_q + \eta_r)\mathcal{P}^{qr}(x), \tag{B.4}$$

$$P^{qr}(x) = \frac{1}{2}(1 - \eta_q\eta_r)\mathcal{P}^{qr}(x) + \frac{i}{2}(\eta_q + \eta_r)\mathcal{S}^{qr}(x), \tag{B.5}$$

$$V^{qr}_{\mu}(x) = \frac{1}{2}(1 + \eta_q\eta_r)\mathcal{V}^{qr}_{\mu}(x) - \frac{i}{2}(\eta_q - \eta_r)\mathcal{A}^{qr}_{\mu}(x), \tag{B.6}$$

$$A^{qr}_{\mu}(x) = \frac{1}{2}(1 + \eta_q\eta_r)\mathcal{A}^{qr}_{\mu}(x) - \frac{i}{2}(\eta_q - \eta_r)\mathcal{V}^{qr}_{\mu}(x), \tag{B.7}$$

$$T^{qr}_{\mu\nu}(x) = \frac{1}{2}(1 - \eta_q\eta_r)\mathcal{T}^{qr}_{\mu\nu}(x) - \frac{i}{4}(\eta_q + \eta_r)\varepsilon_{\mu\nu\rho\sigma}\mathcal{T}^{qr}_{\rho\sigma}(x). \tag{B.8}$$

Therefore, inverse transformations $\{\psi, \bar{\psi}\} \to \{\chi, \bar{\chi}\}$ read

$$\mathcal{S}^{qr}(x) = \frac{1}{2}(1-\eta_q\eta_r)S^{qr}(x) - \frac{i}{2}(\eta_q+\eta_r)P^{qr}(x), \tag{B.9}$$

$$\mathcal{P}^{qr}(x) = \frac{1}{2}(1-\eta_q\eta_r)P^{qr}(x) - \frac{i}{2}(\eta_q+\eta_r)S^{qr}(x), \tag{B.10}$$

$$\mathcal{V}^{qr}_{\mu}(x) = \frac{1}{2}(1+\eta_q\eta_r)V^{qr}_{\mu}(x) + \frac{i}{2}(\eta_q-\eta_r)A^{qr}_{\mu}(x), \tag{B.11}$$

$$\mathcal{A}^{qr}_{\mu}(x) = \frac{1}{2}(1+\eta_q\eta_r)A^{qr}_{\mu}(x) + \frac{i}{2}(\eta_q-\eta_r)V^{qr}_{\mu}(x), \tag{B.12}$$

$$\mathcal{T}^{qr}_{\mu\nu}(x) = \frac{1}{2}(1-\eta_q\eta_r)T^{qr}_{\mu\nu}(x) + \frac{i}{4}(\eta_q+\eta_r)\varepsilon_{\mu\nu\rho\sigma}T^{qr}_{\rho\sigma}(x). \tag{B.13}$$

C ERROR ANALYSIS

We present the techniques that we use in our study for error computation. We review the Γ-method [48], a general framework of error analysis for autocorrelated data.

A general primary observable as P_i^α, where i labels the observable and α the ensemble where it is measured. In practice we only have access to a finite set of samples for a given primary observable P_i^α. We call each measurement in the MC chain

$$p_i^\alpha(k), \quad k = 1, \ldots, N_\alpha, \tag{C.1}$$

where k is each MC measurement and N_α is the total number of measurements on that ensemble. For each observable the mean and the deviation can be estimated

$$\overline{p}_i^\alpha = \frac{1}{N_\alpha} \sum_{k=1}^{N_\alpha} p_i^\alpha(k), \tag{C.2}$$

$$\overline{\delta}_i^\alpha = \overline{p}_i^\alpha - P_i^\alpha. \tag{C.3}$$

$\overline{p}_i^\alpha$ is an unbiased estimators of P_i^α, therefore $\langle \overline{\delta}_i^\alpha \rangle = 0$. We define the function $\Gamma_{ij}^{\alpha\beta}(k)$

$$\langle (p_i^\alpha(k) - P_i^\alpha)(p_j^\beta(k+t) - P_j^\beta) \rangle \equiv \delta_{\alpha\beta} \Gamma_{ij}(k). \tag{C.4}$$

Since, the MC chain is invariant under translations the Γ-function only depends on distance differences.

In order to analyze the statistical error for each observable, we recall the Central Limit Theorem. For a sufficiently large number of samples N_α, the values of $\overline{p}_i^\alpha$ are Gaussian distributed. The Gaussian distribution is defined by the covariance matrix

$$\langle \overline{\delta}_i^\alpha \overline{\delta}_j^\beta \rangle = \frac{1}{N_\alpha^2} \delta_{\alpha\beta} \sum_{kl}^{N_\alpha} \Gamma_{ij}(k-l) = \frac{1}{N_\alpha} C_{ij} \delta_{\alpha\beta}, \tag{C.5}$$

where the covariance matrix can be identified with

$$C_{ij} = \sum_{k=-\infty}^{\infty} \Gamma_{ij}(k). \tag{C.6}$$

The estimator for the Γ-function will take the form

$$\begin{aligned} \overline{\Gamma}_{ij}^{\alpha\beta}(t) &= \frac{1}{N_\alpha - t}\delta_{\alpha\beta}\sum_{k=1}^{N_\alpha - t}\hat{\delta}_i^\alpha(t+k)\hat{\delta}_j^\alpha(k), \\ \hat{\delta}_i^\alpha(k) &= p_i^\alpha(k) - \overline{p}_i^\alpha, \end{aligned} \tag{C.7}$$

where $\hat{\delta}_j(k)$ are the deviations of each measurement with respect to the mean. Therefore, the statistical error for a primary observable for each ensemble can be estimated

$$(\sigma_i^\alpha)^2 = \frac{1}{N_\alpha}\sum_{t=-\infty}^{\infty}\overline{\Gamma}_{ii}^{\alpha\alpha}(t). \tag{C.8}$$

A derived quantity is defined through the application of a a given function f to an observable. The error propagation is based on a Taylor expansion provided that the observable is precise enough and the $\overline{\delta}_i^\alpha(k)$ is small. We define the value of the function f applied to the observable P_i^α.

$$F = f(P_i^\alpha). \tag{C.9}$$

Therefore, the estimator $\overline{F} = f(\overline{p}_i^\alpha)$ can be expanded around F

$$\overline{F} = F + \partial_i^\alpha(f)\,\overline{\delta}_i^\alpha + \frac{1}{2}\partial_i^\alpha\partial_j^\beta(f)\,\overline{\delta}_i^\alpha\overline{\delta}_j^\beta + \dots \tag{C.10}$$

The error of $\overline{F}$ for a given ensemble is computed

$$(\sigma_F)^2 = \langle(\overline{F} - F)^2\rangle \simeq \sum_\alpha \frac{1}{N_\alpha}\sum_{ij}\partial_i^\alpha f\partial_j^\alpha f\sum_t \overline{\Gamma}_{ij}^{\alpha\alpha}(t). \tag{C.11}$$

The integrated autocorrelation time for a derived observable F is defined as

$$\tau_{\text{int}}^\alpha(F) = \frac{1}{2} + \sum_{t=1}^{\infty}\frac{\overline{\Gamma}_F^\alpha(t)}{\overline{\Gamma}_F^\alpha(0)}, \tag{C.12}$$

$$\overline{\Gamma}_F^\alpha(t) = \sum_{ij}\partial_i^\alpha f\,\partial_j^\alpha f\,\overline{\Gamma}_{ij}^{\alpha\alpha}(t). \tag{C.13}$$

The quantity $\tau_{\text{int}}^\alpha(F)$ measures the effective number of independent samples in the MC chain for a given ensemble and a given derived observable F.

In practice, the determinations of the errors and the integrated autocorrelation times requires a truncation in the time series. The correlation between MC trajectories decays exponentially with the MC time. Hence, the autocorrelation function $\Gamma(t) \overset{t\to\infty}{\sim} e^{-t/\tau}$ asymptotically vanishes, whereas its error keeps almost constant. So, the signal

to noise ratio of $\Gamma(t)$ deteriorates significantly. A truncation window is needed to avoid that measurements with large noise dominates the summation.

The summation window W_F^α introduce a bias in the error estimation. As shown in [48]. The systematic uncertainty can be estimated

$$\frac{\delta_{\text{sys}}^\alpha}{\sigma^\alpha} \sim -\exp(-W^\alpha/\tau). \tag{C.14}$$

The summation window has to be chosen larger enough to guarantee that the systematic effect is under control. However, as the window increases the points with larger relative errors are added. The statistical error of the autocorrelation function is

$$\frac{(\delta_{\text{stat}}^\alpha)^2}{(\sigma^\alpha)^2} \simeq \frac{2(2W^\alpha+1)}{N}. \tag{C.15}$$

In order to find the optimal summation window, choose the value that minimizes the sum of the systematic and statistical contributions.

$$W_F^\alpha = \min_W \left(\exp(-W/(S_\tau \tau_{\text{int}})) + \sqrt{\frac{2(2W+1)}{N_\alpha}} \right), \tag{C.16}$$

where S_τ is a parameter that can be tuned to modify the summation window. The value of the parameter must be chosen according to the shape of the autocorrelation function.

The integrated autocorrelation time and the error estimate are estimated

$$\tau_{\text{int}}^\alpha(F) = \frac{1}{2} + \sum_{t=1}^{W_F^\alpha} \frac{\overline{\Gamma}_F^\alpha(t)}{\overline{\Gamma}_F^\alpha(0)}, \tag{C.17}$$

$$(\sigma_F)^2 = \sum_\alpha \frac{2\tau_{\text{int}}^\alpha(F)}{N_\alpha} \overline{\Gamma}_F^\alpha(0). \tag{C.18}$$

Autocorrelation functions decays asymptotically $\Gamma(t) \overset{t\to\infty}{\sim} e^{-t/\tau_{\text{exp}}}$. The exponential autocorrelation time τ_{exp} represents the slowest mode of the transition matrix. The quantity τ_{exp} characterizes the MC chain and is observable independent. In practice, the optimal summation windows are not large enough to resolve the slowest decay mode τ_{exp}. As proposed in [19], the integrated autocorrelation time can be improved to include information about the exponential autocorrelation time

$$\tau_{\text{int}}^\alpha(F) = \frac{1}{2} + \sum_{t=1}^{W_F^\alpha} \frac{\overline{\Gamma}_F^\alpha(t)}{\overline{\Gamma}_F^\alpha(0)} + \tau_{\text{exp}} \frac{\overline{\Gamma}_F^\alpha(W_F^\alpha+1)}{\overline{\Gamma}_F^\alpha(0)}. \tag{C.19}$$

The error is estimated with the previous expression in Eq. (C.18).

The value of τ_{exp} is computed by analyzing cheap simulations with large MC chains. We use the value given in [2] for CLS ensembles

$$\tau_{\text{exp}} = 14(3)\frac{t_0}{a^2}. \tag{C.20}$$

D SYSTEMATIC ERRORS

Systematic effects for each observable are computed using a Bayesian model average [50], where each model is weighted by the Akaike Information Criteria (AIC) [99]. The AIC is defined with the corrected χ^2 for each model M_i such as

$$AIC(M_i) = (\chi^2_{\text{corr}}(M_i)) + 2k_i, \quad (i = 1, \ldots, N_M), \tag{D.1}$$

where k_i is number of parameters of a given model M_i. The weight of each model w_i can be extracted from the AIC in the following way

$$w_i = \mathcal{N} \exp(-\frac{1}{2} AIC(M_i)), \quad \mathcal{N}^{-1} = \sum_{i=1}^{N_M} \exp(-\frac{1}{2} AIC(M_i)). \tag{D.2}$$

Therefore, the Bayesian model average reads

$$\langle \mathcal{O}_c \rangle = \sum_{i=1}^{N_M} w_i \langle \mathcal{O}_c \rangle_i , \tag{D.3}$$

where $\langle \mathcal{O}_c \rangle_i$ are the results of an observable $\mathcal{O}_c$ with a given model M_i. We use the variance of the model average to estimate the systematic error given by the model choice

$$\sigma^2_{\text{sys}}(\mathcal{O}_c) = \langle \mathcal{O}_c^2 \rangle - \langle \mathcal{O}_c \rangle^2 = \sum_{i=1}^{N_M} w_i \langle \mathcal{O}_c \rangle_i^2 - \left(\sum_{i=1}^{N_M} w_i \langle \mathcal{O}_c \rangle_i \right)^2 . \tag{D.4}$$

E ADDITIONAL PLOTS

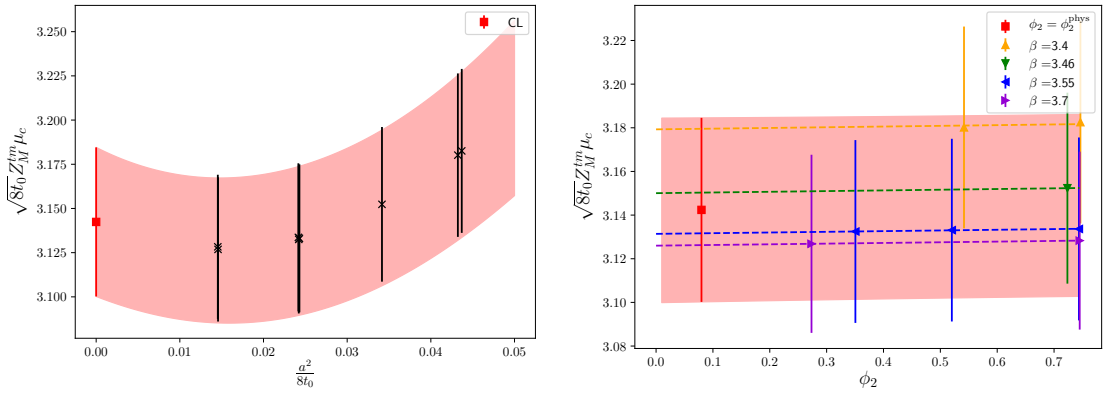

Figure E.1: *Left*: Continuum limit extrapolation of the RGI charm quark mass $M_c^{\text{RGI}}(N_f = 3)$ in terms of the reference scale t_0. The red band represent the projection to the physical point $\phi_2 = \phi_2^{\text{phys}}$ and $\phi_c = \phi_c^{\text{phys}}$. *Right*: Chiral extrapolation of the RGI charm quark mass $M_c^{\text{RGI}}(N_f = 3)$ in terms of the reference scale t_0. The red band represents the projection to the continuum limit. Dashed lines correspond to chiral extrapolations at finite lattice spacing. The results of both plots are matched to $\phi_{c,3}^{\text{phys}}$.

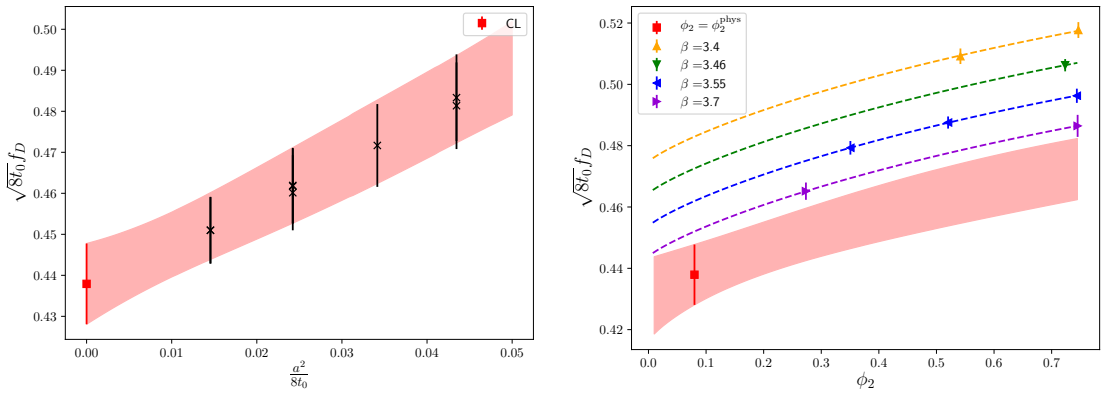

Figure E.2: *Left*: Continuum limit extrapolation of the decay constant f_D in units of the reference scale t_0. The red band represent the projection to the physical point $\phi_2 = \phi_2^{\text{phys}}$ and $\phi_c = \phi_c^{\text{phys}}$. *Right*: Chiral extrapolation of the decay constant f_D in units of the reference scale t_0. The red band represents the projection to the continuum limit. Dashed lines correspond to chiral extrapolations at finite lattice spacing. The results of both plots are matched to $\phi_{c,2}^{\text{phys}}$.

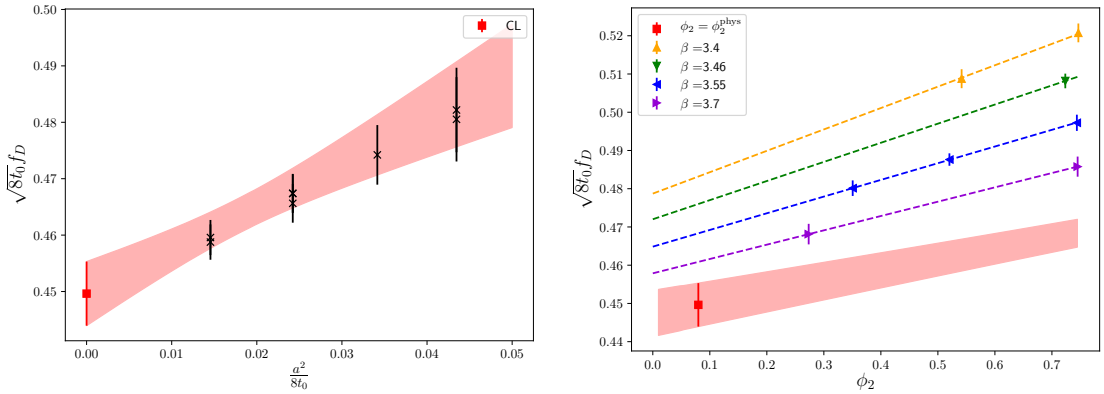

Figure E.3: *Left*: Continuum limit extrapolation of the decay constant f_D in units of the reference scale t_0. The red band represent the projection to the physical point $\phi_2 = \phi_2^{\text{phys}}$ and $\phi_c = \phi_c^{\text{phys}}$. *Right*: Chiral extrapolation of the decay constant f_D in units of the reference scale t_0. The red band represents the projection to the continuum limit. Dashed lines correspond to chiral extrapolations at finite lattice spacing. The results of both plots are matched to $\phi_{c,3}^{\text{phys}}$.

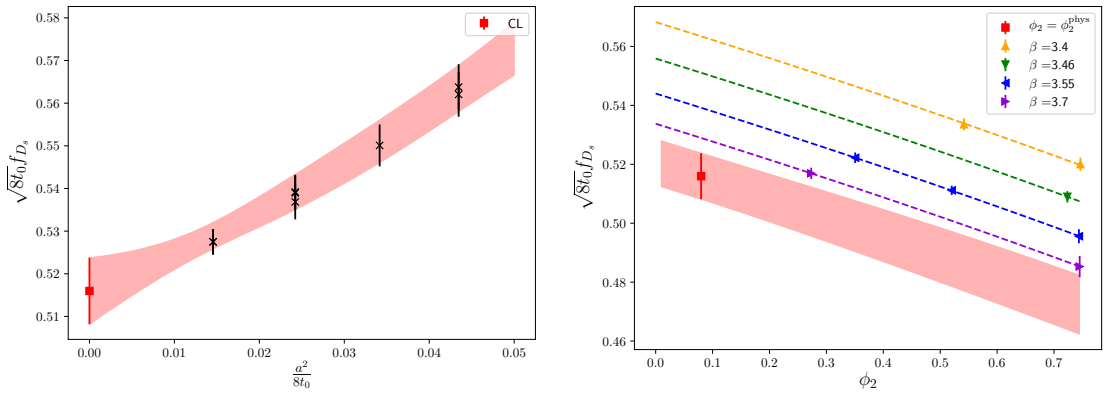

Figure E.4: *Left*: Continuum limit extrapolation of the decay constant f_{D_s} in units of the reference scale t_0. The red band represent the projection to the physical point $\phi_2 = \phi_2^{\rm phys}$ and $\phi_c = \phi_c^{\rm phys}$. *Right*: Chiral extrapolation of the decay constant f_{D_s} in units of the reference scale t_0. The red band represents the projection to the continuum limit. Dashed lines correspond to chiral extrapolations at finite lattice spacing. The results of both plots are matched to $\phi_{c,2}^{\rm phys}$.

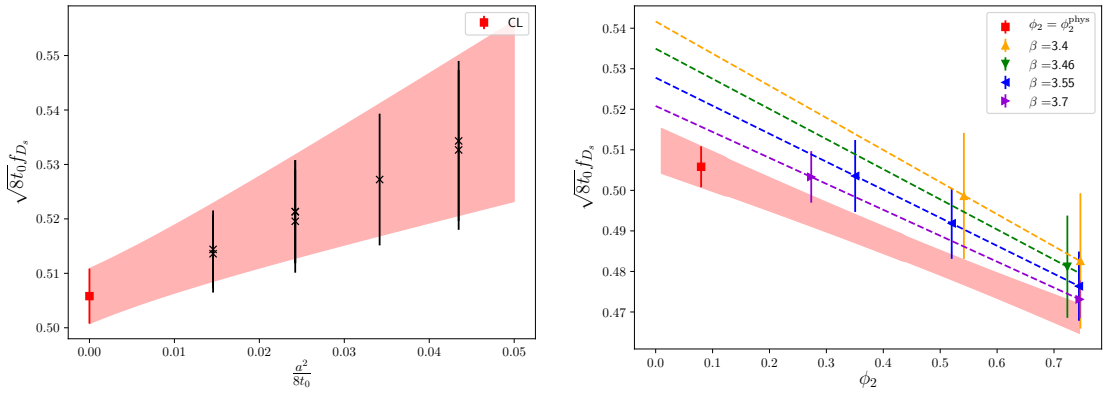

Figure E.5: *Left*: Continuum limit extrapolation of the decay constant f_{D_s} in units of the reference scale t_0. The red band represent the projection to the physical point $\phi_2 = \phi_2^{\rm phys}$ and $\phi_c = \phi_c^{\rm phys}$. *Right*: Chiral extrapolation of the decay constant f_{D_s} in units of the reference scale t_0. The red band represents the projection to the continuum limit. Dashed lines correspond to chiral extrapolations at finite lattice spacing. The results of both plots are matched to $\phi_{c,3}^{\rm phys}$.

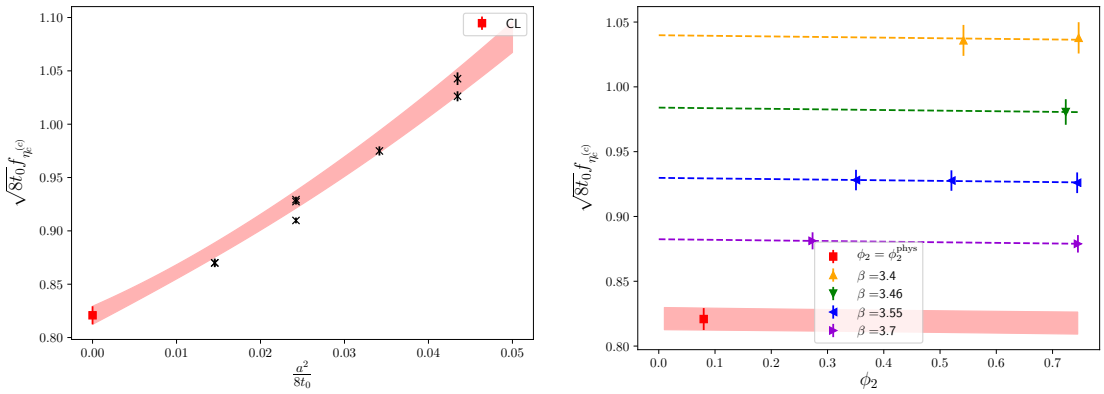

Figure E.6: *Left*: Continuum limit extrapolation of the decay constant f_{η_c} in units of the reference scale t_0. The red band represent the projection to the physical point $\phi_2 = \phi_2^{\text{phys}}$ and $\phi_c = \phi_c^{\text{phys}}$. *Right*: Chiral extrapolation of the decay constant f_{η_c} in units of the reference scale t_0. The red band represents the projection to the continuum limit. Dashed lines correspond to chiral extrapolations at finite lattice spacing. The results of both plots are matched to $\phi_{c,2}^{\text{phys}}$.

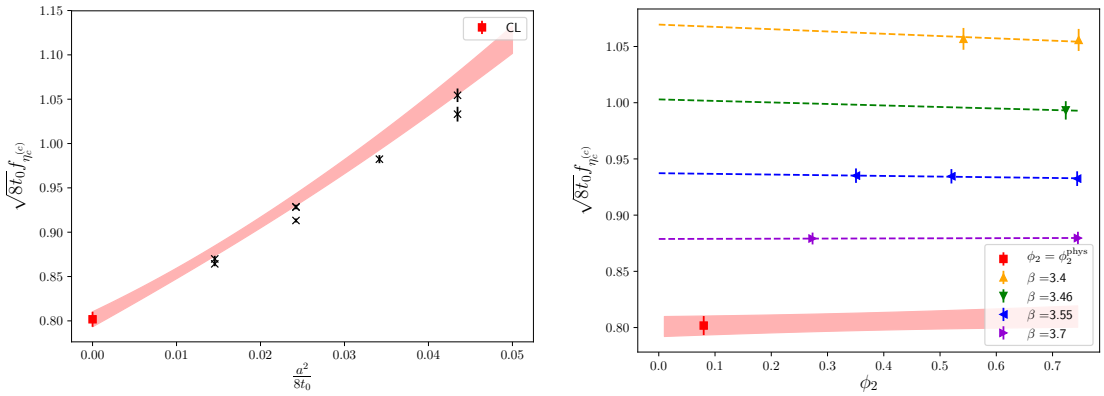

Figure E.7: *Left*: Continuum limit extrapolation of the decay constant f_{η_c} in units of the reference scale t_0. The red band represent the projection to the physical point $\phi_2 = \phi_2^{\text{phys}}$ and $\phi_c = \phi_c^{\text{phys}}$. *Right*: Chiral extrapolation of the decay constant f_{η_c} in units of the reference scale t_0. The red band represents the projection to the continuum limit. Dashed lines correspond to chiral extrapolations at finite lattice spacing. The results of both plots are matched to $\phi_{c,3}^{\text{phys}}$.

BIBLIOGRAPHY

[1] K. G. Wilson, "Confinement of Quarks," *Phys. Rev. D*, vol. 10, pp. 2445–2459, 1974.

[2] M. Bruno *et al.*, "Simulation of QCD with $N_f = 2 + 1$ flavors of non-perturbatively improved Wilson fermions," *JHEP*, vol. 02, p. 043, 2015.

[3] A. Ramos, "Automatic differentiation for error analysis of Monte Carlo data," *Comput. Phys. Commun.*, vol. 238, pp. 19–35, 2019.

[4] M. Luscher and P. Weisz, "Computation of the Action for On-Shell Improved Lattice Gauge Theories at Weak Coupling," *Phys. Lett. B*, vol. 158, pp. 250–254, 1985.

[5] H. Nielsen and M. Ninomiya, "A no-go theorem for regularizing chiral fermions," *Physics Letters B*, vol. 105, no. 2, pp. 219–223, 1981.

[6] K. G. Wilson, "Quarks and Strings on a Lattice," in *13th International School of Subnuclear Physics: New Phenomena in Subnuclear Physics*, 11 1975.

[7] L. Del Debbio, L. Giusti, M. Luscher, R. Petronzio, and N. Tantalo, "Stability of lattice QCD simulations and the thermodynamic limit," *JHEP*, vol. 02, p. 011, 2006.

[8] R. Frezzotti, P. A. Grassi, S. Sint, and P. Weisz, "Lattice QCD with a chirally twisted mass term," *JHEP*, vol. 08, p. 058, 2001.

[9] A. Shindler, "Twisted mass lattice QCD," *Phys. Rept.*, vol. 461, pp. 37–110, 2008.

[10] K. Symanzik, "Continuum Limit and Improved Action in Lattice Theories. 1. Principles and phi**4 Theory," *Nucl. Phys. B*, vol. 226, pp. 187–204, 1983.

[11] K. Symanzik, "Continuum Limit and Improved Action in Lattice Theories. 2. O(N) Nonlinear Sigma Model in Perturbation Theory," *Nucl. Phys. B*, vol. 226, pp. 205–227, 1983.

[12] M. Bochicchio, L. Maiani, G. Martinelli, G. C. Rossi, and M. Testa, "Chiral Symmetry on the Lattice with Wilson Fermions," *Nucl. Phys. B*, vol. 262, p. 331, 1985.

[13] B. Sheikholeslami and R. Wohlert, "Improved Continuum Limit Lattice Action for QCD with Wilson Fermions," *Nucl. Phys. B*, vol. 259, p. 572, 1985.

[14] R. Frezzotti and G. C. Rossi, "Chirally improving Wilson fermions. 1. O(a) improvement," *JHEP*, vol. 08, p. 007, 2004.

[15] R. Frezzotti and G. C. Rossi, "Chirally improving Wilson fermions. II. Four-quark operators," *JHEP*, vol. 10, p. 070, 2004.

[16] M. Bruno, T. Korzec, and S. Schaefer, "Setting the scale for the CLS $2 + 1$ flavor ensembles," *Phys. Rev. D*, vol. 95, no. 7, p. 074504, 2017.

[17] J. A. Romero Jurado, *Study of mesonic observables from a mixed action lattice QCD formalism.* PhD thesis, Madrid, Autonoma U., 2020.

[18] J. Bulava and S. Schaefer, "Improvement of $N_f = 3$ lattice QCD with Wilson fermions and tree-level improved gauge action," *Nucl. Phys. B*, vol. 874, pp. 188–197, 2013.

[19] S. Schaefer, R. Sommer, and F. Virotta, "Critical slowing down and error analysis in lattice QCD simulations," *Nucl. Phys. B*, vol. 845, pp. 93–119, 2011.

[20] M. Luscher, "Topology of Lattice Gauge Fields," *Commun. Math. Phys.*, vol. 85, p. 39, 1982.

[21] M. Bruno, S. Schaefer, and R. Sommer, "Topological susceptibility and the sampling of field space in $\mathrm{N}_f = 2$ lattice QCD simulations," *JHEP*, vol. 08, p. 150, 2014.

[22] M. Luscher, "Topology, the Wilson flow and the HMC algorithm," *PoS*, vol. LATTICE2010, p. 015, 2010.

[23] M. Luscher and S. Schaefer, "Lattice QCD without topology barriers," *JHEP*, vol. 07, p. 036, 2011.

[24] D. Becirevic, P. Boucaud, V. Lubicz, G. Martinelli, F. Mescia, S. Simula, and C. Tarantino, "Exploring twisted mass lattice QCD with the Clover term," *Phys. Rev. D*, vol. 74, p. 034501, 2006.

[25] P. Dimopoulos, H. Simma, and A. Vladikas, "Quenched B(K)-parameter from Osterwalder-Seiler tmQCD quarks and mass-splitting discretization effects," *JHEP*, vol. 07, p. 007, 2009.

[26] A. Bussone, S. Chaves, G. Herdoíza, C. Pena, D. Preti, J. A. Romero, and J. Ugarrio, "Heavy-quark physics with a tmQCD valence action," *PoS*, vol. LATTICE2018, p. 270, 2019.

[27] K. Osterwalder and E. Seiler, "Gauge Field Theories on the Lattice," *Annals Phys.*, vol. 110, p. 440, 1978.

[28] A. Bussone, G. Herdoíza, C. Pena, D. Preti, J. A. Romero, and J. Ugarrio, "Matching of $N_f = 2 + 1$ CLS ensembles to a tmQCD valence sector," *PoS*, vol. LATTICE2018, p. 318, 2019.

[29] A. Bussone, A. Conigli, G. Herdoíza, J. Frison, C. Pena, D. Preti, J. A. Romero, A. Sáez, and J. Ugarrio, "Light meson physics and scale setting from mixed action with Wilson twisted mass valence quarks," in *38th International Symposium on Lattice Field Theory*, 2021.

[30] S. Duane, A. D. Kennedy, B. J. Pendleton, and D. Roweth, "Hybrid Monte Carlo," *Phys. Lett. B*, vol. 195, pp. 216–222, 1987.

[31] G. M. de Divitiis, R. Petronzio, and N. Tantalo, "Distance preconditioning for lattice Dirac operators," *Phys. Lett. B*, vol. 692, pp. 157–160, 2010.

[32] M. Lüscher, "Properties and uses of the Wilson flow in lattice QCD," *JHEP*, vol. 08, p. 071, 2010. [Erratum: JHEP 03, 092 (2014)].

[33] A. D. Kennedy and P. Rossi, "CLASSICAL MECHANICS ON GROUP MANIFOLDS AND APPLICATIONS TO HYBRID MONTE CARLO," *Nucl. Phys. B*, vol. 327, pp. 782–790, 1989.

[34] J. C. Sexton and D. H. Weingarten, "Hamiltonian evolution for the hybrid Monte Carlo algorithm," *Nucl. Phys. B*, vol. 380, pp. 665–677, 1992.

[35] I. Omelyan, I. Mryglod, and R. Folk, "Symplectic analytically integrable decomposition algorithms: classification, derivation, and application to molecular dynamics, quantum and celestial mechanics simulations," *Computer Physics Communications*, vol. 151, no. 3, pp. 272–314, 2003.

[36] M. Luscher and F. Palombi, "Fluctuations and reweighting of the quark determinant on large lattices," *PoS*, vol. LATTICE2008, p. 049, 2008.

[37] M. A. Clark and A. D. Kennedy, "Accelerating dynamical fermion computations using the rational hybrid Monte Carlo (RHMC) algorithm with multiple pseudofermion fields," *Phys. Rev. Lett.*, vol. 98, p. 051601, 2007.

[38] A. D. Kennedy, I. Horvath, and S. Sint, "A New exact method for dynamical fermion computations with nonlocal actions," *Nucl. Phys. B Proc. Suppl.*, vol. 73, pp. 834–836, 1999.

[39] M. Hasenbusch, "Speeding up the hybrid Monte Carlo algorithm for dynamical fermions," *Phys. Lett. B*, vol. 519, pp. 177–182, 2001.

[40] M. Hasenbusch and K. Jansen, "Speeding up lattice QCD simulations with clover improved Wilson fermions," *Nucl. Phys. B*, vol. 659, pp. 299–320, 2003.

[41] T. A. DeGrand, "A Conditioning Technique for Matrix Inversion for Wilson Fermions," *Comput. Phys. Commun.*, vol. 52, pp. 161–164, 1988.

[42] J. Viehoff, N. Eicker, S. Gusken, H. Hoeber, P. Lacock, T. Lippert, K. Schilling, A. Spitz, and P. Uberholz, "Improving stochastic estimator techniques for disconnected diagrams," *Nucl. Phys. B Proc. Suppl.*, vol. 63, pp. 269–271, 1998.

[43] J. Foley, K. Jimmy Juge, A. O'Cais, M. Peardon, S. M. Ryan, and J.-I. Skullerud, "Practical all-to-all propagators for lattice QCD," *Comput. Phys. Commun.*, vol. 172, pp. 145–162, 2005.

[44] M. Luscher, "Trivializing maps, the Wilson flow and the HMC algorithm," *Commun. Math. Phys.*, vol. 293, pp. 899–919, 2010.

[45] M. Luscher and P. Weisz, "Perturbative analysis of the gradient flow in non-abelian gauge theories," *JHEP*, vol. 02, p. 051, 2011.

[46] I. Campos, P. Fritzsch, C. Pena, D. Preti, A. Ramos, and A. Vladikas, "Non-perturbative quark mass renormalisation and running in $N_f = 3$ QCD," *Eur. Phys. J. C*, vol. 78, no. 5, p. 387, 2018.

[47] J. Heitger, F. Joswig, and S. Kuberski, "Determination of the charm quark mass in lattice QCD with $2 + 1$ flavours on fine lattices," *JHEP*, vol. 05, p. 288, 2021.

[48] U. Wolff, "Monte Carlo errors with less errors," *Comput. Phys. Commun.*, vol. 156, pp. 143–153, 2004. [Erratum: Comput.Phys.Commun. 176, 383 (2007)].

[49] J. Revels, M. Lubin, and T. Papamarkou, "Forward-mode automatic differentiation in julia," *CoRR*, vol. abs/1607.07892, 2016.

[50] W. I. Jay and E. T. Neil, "Bayesian model averaging for analysis of lattice field theory results," *Phys. Rev. D*, vol. 103, p. 114502, 2021.

[51] S. Aoki *et al.*, "Review of lattice results concerning low-energy particle physics," *Eur. Phys. J. C*, vol. 77, no. 2, p. 112, 2017.

[52] H. Georgi, "An Effective Field Theory for Heavy Quarks at Low-energies," *Phys. Lett. B*, vol. 240, pp. 447–450, 1990.

[53] P. A. Zyla *et al.*, "Review of Particle Physics," *PTEP*, vol. 2020, no. 8, p. 083C01, 2020.

[54] B. Grinstein, E. E. Jenkins, A. V. Manohar, M. J. Savage, and M. B. Wise, "Chiral perturbation theory for f D(s) / f D and B B(s) / B B," *Nucl. Phys. B*, vol. 380, pp. 369–376, 1992.

[55] J. L. Goity, "Chiral perturbation theory for SU(3) breaking in heavy meson systems," *Phys. Rev. D*, vol. 46, pp. 3929–3936, 1992.

[56] C. Michael, "Fitting correlated data," *Phys. Rev. D*, vol. 49, pp. 2616–2619, 1994.

[57] C. Michael and A. McKerrell, "Fitting correlated hadron mass spectrum data," *Phys. Rev. D*, vol. 51, pp. 3745–3750, 1995.

[58] M. Bruno and R. Sommer In preparation.

[59] K. G. Chetyrkin, J. H. Kuhn, and M. Steinhauser, "RunDec: A Mathematica package for running and decoupling of the strong coupling and quark masses," *Comput. Phys. Commun.*, vol. 133, pp. 43–65, 2000.

[60] B. Schmidt and M. Steinhauser, "CRunDec: a C++ package for running and decoupling of the strong coupling and quark masses," *Comput. Phys. Commun.*, vol. 183, pp. 1845–1848, 2012.

[61] F. Herren and M. Steinhauser, "Version 3 of RunDec and CRunDec," *Comput. Phys. Commun.*, vol. 224, pp. 333–345, 2018.

[62] Y. Aoki *et al.*, "FLAG Review 2021," 11 2021.

[63] C. McNeile, C. T. H. Davies, E. Follana, K. Hornbostel, and G. P. Lepage, "High-Precision c and b Masses, and QCD Coupling from Current-Current Correlators in Lattice and Continuum QCD," *Phys. Rev. D*, vol. 82, p. 034512, 2010.

[64] K. Nakayama, B. Fahy, and S. Hashimoto, "Short-distance charmonium correlator on the lattice with Möbius domain-wall fermion and a determination of charm quark mass," *Phys. Rev. D*, vol. 94, no. 5, p. 054507, 2016.

[65] Y.-B. Yang *et al.*, "Charm and strange quark masses and f_{D_s} from overlap fermions," *Phys. Rev. D*, vol. 92, no. 3, p. 034517, 2015.

[66] P. A. Boyle, L. Del Debbio, A. Jüttner, A. Khamseh, F. Sanfilippo, and J. T. Tsang, "The decay constants $\mathbf{f_D}$ and $\mathbf{f_{D_s}}$ in the continuum limit of $\mathbf{N_f = 2 + 1}$ domain wall lattice QCD," *JHEP*, vol. 12, p. 008, 2017.

[67] H. Na, C. T. H. Davies, E. Follana, G. P. Lepage, and J. Shigemitsu, "$|V_{cd}|$ from D Meson Leptonic Decays," *Phys. Rev. D*, vol. 86, p. 054510, 2012.

[68] C. Alexandrou *et al.*, "Quark masses using twisted-mass fermion gauge ensembles," *Phys. Rev. D*, vol. 104, no. 7, p. 074515, 2021.

[69] D. Hatton, C. T. H. Davies, B. Galloway, J. Koponen, G. P. Lepage, and A. T. Lytle, "Charmonium properties from lattice QCD+QED : Hyperfine splitting, J/ψ leptonic width, charm quark mass, and a_μ^c," *Phys. Rev. D*, vol. 102, no. 5, p. 054511, 2020.

[70] A. T. Lytle, C. T. H. Davies, D. Hatton, G. P. Lepage, and C. Sturm, "Determination of quark masses from $\mathbf{n_f = 4}$ lattice QCD and the RI-SMOM intermediate scheme," *Phys. Rev. D*, vol. 98, no. 1, p. 014513, 2018.

[71] A. Bazavov *et al.*, "Up-, down-, strange-, charm-, and bottom-quark masses from four-flavor lattice QCD," *Phys. Rev. D*, vol. 98, no. 5, p. 054517, 2018.

[72] B. Chakraborty, C. T. H. Davies, B. Galloway, P. Knecht, J. Koponen, G. C. Donald, R. J. Dowdall, G. P. Lepage, and C. McNeile, "High-precision quark masses and QCD coupling from $n_f = 4$ lattice QCD," *Phys. Rev. D*, vol. 91, no. 5, p. 054508, 2015.

[73] C. Alexandrou, V. Drach, K. Jansen, C. Kallidonis, and G. Koutsou, "Baryon spectrum with $N_f = 2 + 1 + 1$ twisted mass fermions," *Phys. Rev. D*, vol. 90, no. 7, p. 074501, 2014.

[74] N. Carrasco *et al.*, "Up, down, strange and charm quark masses with N_f = 2+1+1 twisted mass lattice QCD," *Nucl. Phys. B*, vol. 887, pp. 19–68, 2014.

[75] P. Petreczky and J. H. Weber, "Strong coupling constant and heavy quark masses in (2+1)-flavor QCD," *Phys. Rev. D*, vol. 100, no. 3, p. 034519, 2019.

[76] Y. Maezawa and P. Petreczky, "Quark masses and strong coupling constant in 2+1 flavor QCD," *Phys. Rev. D*, vol. 94, no. 3, p. 034507, 2016.

[77] I. Allison *et al.*, "High-Precision Charm-Quark Mass from Current-Current Correlators in Lattice and Continuum QCD," *Phys. Rev. D*, vol. 78, p. 054513, 2008.

[78] A. Bazavov *et al.*, "Charmed and Light Pseudoscalar Meson Decay Constants from Four-Flavor Lattice QCD with Physical Light Quarks," *Phys. Rev. D*, vol. 90, no. 7, p. 074509, 2014.

[79] A. Bazavov *et al.*, "B- and D-meson leptonic decay constants from four-flavor lattice QCD," *Phys. Rev. D*, vol. 98, no. 7, p. 074512, 2018.

[80] N. Carrasco *et al.*, "Leptonic decay constants f_K, f_D, and f_{D_s} with $N_f = 2+1+1$ twisted-mass lattice QCD," *Phys. Rev. D*, vol. 91, no. 5, p. 054507, 2015.

[81] P. Dimopoulos, R. Frezzotti, P. Lami, V. Lubicz, E. Picca, L. Riggio, G. C. Rossi, F. Sanfilippo, S. Simula, and C. Tarantino, "Pseudoscalar decay constants f_K/f_π, f_D and f_{D_s} with $N_f = 2+1+1$ ETMC configurations," *PoS*, vol. LATTICE2013, p. 314, 2014.

[82] A. Bazavov *et al.*, "Charmed and Strange Pseudoscalar Meson Decay Constants from HISQ Simulations," *PoS*, vol. LATTICE2013, p. 405, 2014.

[83] A. Bazavov *et al.*, "Pseudoscalar meson physics with four dynamical quarks," *PoS*, vol. LATTICE2012, p. 159, 2012.

[84] Y. Chen, W.-F. Chiu, M. Gong, Z. Liu, and Y. Ma, "Charmed and ϕ meson decay constants from 2+1-flavor lattice QCD," *Chin. Phys. C*, vol. 45, no. 2, p. 023109, 2021.

[85] P. A. Boyle, L. Del Debbio, N. Garron, A. Juttner, A. Soni, J. T. Tsang, and O. Witzel, "SU(3)-breaking ratios for $D_{(s)}$ and $B_{(s)}$ mesons," 12 2018.

[86] A. Bazavov *et al.*, "B- and D-meson decay constants from three-flavor lattice QCD," *Phys. Rev. D*, vol. 85, p. 114506, 2012.

[87] Y. Namekawa *et al.*, "Charm quark system at the physical point of 2+1 flavor lattice QCD," *Phys. Rev. D*, vol. 84, p. 074505, 2011.

[88] C. T. H. Davies, C. McNeile, E. Follana, G. P. Lepage, H. Na, and J. Shigemitsu, "Update: Precision D_s decay constant from full lattice QCD using very fine lattices," *Phys. Rev. D*, vol. 82, p. 114504, 2010.

[89] E. Follana, C. T. H. Davies, G. P. Lepage, and J. Shigemitsu, "High Precision determination of the pi, K, D and D(s) decay constants from lattice QCD," *Phys. Rev. Lett.*, vol. 100, p. 062002, 2008.

[90] C. Aubin *et al.*, "Charmed meson decay constants in three-flavor lattice QCD," *Phys. Rev. Lett.*, vol. 95, p. 122002, 2005.

[91] R. Balasubramamian and B. Blossier, "Decay constant of B_s and B_s^* mesons from $\mathrm{N_f} = 2$ lattice QCD," *Eur. Phys. J. C*, vol. 80, no. 5, p. 412, 2020.

[92] B. Blossier, J. Heitger, and M. Post, "Leptonic D_s decays in two-flavour lattice QCD," *Phys. Rev. D*, vol. 98, no. 5, p. 054506, 2018.

[93] W.-P. Chen, Y.-C. Chen, T.-W. Chiu, H.-Y. Chou, T.-S. Guu, and T.-H. Hsieh, "Decay Constants of Pseudoscalar D-mesons in Lattice QCD with Domain-Wall Fermion," *Phys. Lett. B*, vol. 736, pp. 231–236, 2014.

[94] J. Heitger, G. M. von Hippel, S. Schaefer, and F. Virotta, "Charm quark mass and D-meson decay constants from two-flavour lattice QCD," *PoS*, vol. LATTICE2013, p. 475, 2014.

[95] N. Carrasco *et al.*, "B-physics from $N_f = 2$ tmQCD: the Standard Model and beyond," *JHEP*, vol. 03, p. 016, 2014.

[96] P. Dimopoulos *et al.*, "Lattice QCD determination of m_b, f_B and f_{Bs} with twisted mass Wilson fermions," *JHEP*, vol. 01, p. 046, 2012.

[97] B. Blossier *et al.*, "Pseudoscalar decay constants of kaon and D-mesons from $N_f = 2$ twisted mass Lattice QCD," *JHEP*, vol. 07, p. 043, 2009.

[98] A. Bussone, A. Conigli, J. Frison, G. Herdoíza, C. Pena, D. Preti, J. A. Romero, and J. Ugarrio, "Charm physics with a tmQCD mixed action," in *38th International Symposium on Lattice Field Theory*, 12 2021.

[99] H. Akaike, "A bayesian analysis of the minimum aic procedure," *Annals of the Institute of Statistical Mathematics*, vol. 30, pp. 9–14, Dec 1978.